Domain-wall excitations in the two-dimensional Ising spin glass

Hamid Khoshbakht[1,2,*] and Martin Weigel[1,†]

[1]*Applied Mathematics Research Centre, Coventry University, Coventry, CV1 5FB, United Kingdom*
[2]*Institut für Physik, Johannes Gutenberg-Universität Mainz, Staudinger Weg 7, D-55099 Mainz, Germany*

The Ising spin glass in two dimensions exhibits rich behavior with subtle differences in the scaling for different coupling distributions. We use recently developed mappings to graph-theoretic problems together with highly efficient implementations of combinatorial optimization algorithms to determine exact ground states for systems on square lattices with up to $10\,000 \times 10\,000$ spins. While these mappings only work for planar graphs, for example for systems with periodic boundary conditions in at most one direction, we suggest here an iterative windowing technique that allows one to determine ground states for fully periodic samples up to sizes similar to those for the open-periodic case. Based on these techniques, a large number of disorder samples are used together with a careful finite-size scaling analysis to determine the stiffness exponents and domain-wall fractal dimensions with unprecedented accuracy, our best estimates being $\theta = -0.2793(3)$ and $d_{\mathrm{f}} = 1.273\,19(9)$ for Gaussian couplings. For bimodal disorder, a new uniform sampling algorithm allows us to study the domain-wall fractal dimension, finding $d_{\mathrm{f}} = 1.279(2)$. Additionally, we also investigate the distributions of ground-state energies, of domain-wall energies, and domain-wall lengths.

I. INTRODUCTION

The problem of an adequate description and understanding of the behavior of spin systems with strong disorder has been studied for around forty years by a large number of scientists in statistical and condensed matter physics as well as, increasingly, researchers in adjacent fields such as computer science and mathematics [1]. It is a hard problem in that many of the well-developed tools of the theory of critical phenomena, such as the renormalization group, fail to satisfactorily describe all important aspects of these models, and in that the standard techniques of numerical simulations are faced with diminishing efficiency in view of exploding relaxation times and the massive computational demand of the average over quenched disorder. However, it is also a good and fruitful problem in that the questions it poses are deeply rooted in the foundations of statistical mechanics [2] and the simplicity of the models has led to applications ranging from the physics of structural glasses to error correcting codes and neural networks [3].

While even fundamental questions such as the values of the lower and upper critical dimensions of such models are still under active debate [4–8], there is consensus that a spin-glass phase appears at nonzero temperatures for short-ranged systems of Ising spins in at least three dimensions, but no spin-glass order occurs beyond ground states in two-dimensional (2D) systems [9–11]. While such 2D geometries might hence appear less useful for modeling experimentally realized spin-glass phases, the physics of these systems is in fact rather interesting in its own right. One intriguing aspect is that for sufficiently asymmetric coupling distributions a long-range

ferromagnetic phase can exist at nonzero temperatures, and it is found that the phase boundary at low temperatures shows re-entrance or inverse melting, that is, on further cooling a system in the ferromagnetic phase, order is lost in favor of a paramagnetic state [12,13]. Another facet is the question of universality regarding the distribution of exchange couplings; at zero temperature, the bimodal model has extensive ground-state degeneracies leading to behavior rather different from the case of continuous coupling distributions [14]. The resulting entropy of volatile spin clusters was long believed to lead to power-law correlations at zero temperature, but there is now evidence of true long-range spin-glass order [15,16]. The behavior of this model at low temperatures is determined by a delicate interplay of the distinct fixed points of the universality classes of discrete and continuous coupling distributions, respectively [17–20], and there is still no complete consensus about universality at finite temperatures [11,21]. It is the subtle role played by entropic fluctuations, which makes this model relevant to the finite-temperature transitions observed in three dimensions [17].

Apart from such theoretical considerations, interest in the 2D models has been fueled by the relative ease in numerical tractability as compared to higher-dimensional systems. This goes beyond the general advantage of systems in low dimensions of providing larger linear system sizes at the same number of sites: 2D systems in zero external field are an exception to the *NP* hardness of ground-state problems found in systems of higher dimensions [22]. Ground states on planar graphs can be determined in polynomial time from the mapping to a minimum-weight perfect matching problem [23]. This allows to treat significantly larger lattice sizes than those accessible to simulation methods. The restriction to planar graphs, and hence periodic boundary conditions in at most one direction, has been rather inconvenient for certain

*hamidkhoshbakht@gmail.com
†martin.weigel@complexity-coventry.org

types of studies [24] and, in general, leads to relatively larger finite-size corrections. Polynomial-time algorithms also exist for the more general problem of determining the partition function [25–27]. These methods, based on the evaluation of Pfaffians, have the advantage of allowing for periodic boundary conditions, but they are technically more demanding than the ground-state computations and thus restricted to smaller system sizes. Only recent advances have allowed to extend these approaches to system sizes $L \gtrsim 100$ [28]. In parallel, exact sampling techniques for Ising spin glasses at nonzero temperatures based on the application of "coupling-from-the-past" [29] or sampling of dimer coverings [30] have recently been suggested, that are either restricted to or only efficient in 2D [28,31].

A wide range of aspects of 2D spin glasses has been found to be consistent with droplet theory [32–34]. Droplet and domain-wall excitations can be directly inserted in zero-temperature configurations. Domain-wall energies are found to scale as a power law $E_{\text{def}} \sim L^{\theta_{\text{DW}}}$ for the Gaussian model with $\theta_{\text{DW}} \approx -0.28$ [14]. Roughly consistent values are found for the scaling of droplet energies if scaling corrections are taken into account [35]. No power-law scaling of domain-wall energies is found for bimodal couplings [14], but droplets in this model show $\theta \approx -0.29$, possibly compatible with the Gaussian case [36]. As the spin-glass phase is confined to zero temperature for 2D models, ground-state calculations give direct access to the *critical* behavior of the spin-glass transition. In this case, the correlation length exponent is expected to follow from $\nu = -1/\theta$ [33]. As $\eta = 0$ at least for the Gaussian model [11], this is the only relevant critical exponent (but see Ref. [36] for the bimodal case). Domain walls and droplet interfaces are found to be fractal curves with dimension $d_{\text{f}} < 2$, i.e., not space filling [37]. At least for the Gaussian case, these fractal curves appear to be compatible, under certain conditions, with a description in terms of stochastic Loewner evolution [38–40]. Such consistence together with further assumptions would suggest a relation between stiffness exponent and fractal dimension, $d_{\text{f}} = 1 + 3/[4(3 + \theta)]$ [38]. For the bimodal model, on the other hand, the fractal dimension is possibly different [41–43], but calculations are complicated by sampling problems since the ground-state algorithms do not produce the degenerate ground states with the correct weights. These subtle differences between results for different coupling distributions and excitation types call for high-precision studies to distinguish random from systematic coincidences. Some previous results for θ and d_{f} in the Gaussian model are collected in Table I.

Here we combine a formulation of the ground-state problem on planar graphs in terms of Kasteleyn cities [44,45] with a recently suggested efficient implementation of the Blossom algorithm for minimum-weight perfect matching [46]. This allows us to determine ground states for systems of up to 10 000 × 10 000 spins on commodity hardware. To extend these results to the case of periodic boundaries with the smaller scaling corrections expected there, we introduce a hierarchical optimization procedure using windows, alike to the patchwork dynamics discussed in Ref. [47], which allows to determine ground states of fully periodic samples with a constant relative increase in computational effort as compared to the matching technique for planar samples. To treat the case of bimodal couplings cor-

TABLE I. Previous estimates of the spin-stiffness exponent θ and the fractal dimension d_{f} of the 2D Ising spin glass with Gaussian bond distribution.

Ref.	θ	d_{f}	max. system size
[48]	$-0.281(5)$	—	8×8
[49]	$-0.285(2)$	—	30×30
[50]	$-0.294(9)$	—	12×12
[37]	$-0.29(1)$	1.26(3)	120×13
[51]	$-0.281(2)$	1.34(10)	30×30
[14]	$-0.282(2)$	—	480×480
[52]	—	1.25(1)	256×256
[42]	$-0.284(4)$	1.273(3)	256×256
[39]	—	1.28(1)	720×360
[53]	$-0.287(4)$	—	16×1024
[54]	$-0.282(3)$	—	12×384
[55]	$-0.281(7)$	—	64×64
[38]	$-0.285(5)$	1.27(1)	300×300
[41]	$-0.287(4)$	1.274(2)	320×320
This work	$-0.2793(3)$	1.27319(9)	$10\,000 \times 10\,000$

rectly, we use a new approach based on an exact decomposition of the ground-state manifold into rigid clusters that are then sampled within a parallel tempering framework that guarantees uniform sampling of ground states to high precision.

The rest of this paper is organized as follows. In Sec. II, we outline the matching algorithm based on Kasteleyn cities, introduce the windowing technique that allows to generalize the method to systems with fully periodic boundaries, and evaluate the performance of these algorithms. Section III is devoted to the system with Gaussian coupling distribution, and we report our results for the average ground-state and defect energies, the domain-wall fractal dimension as well as the probability distributions of these quantities for different boundary conditions. In Sec. IV, we analyze these quantities for the bimodal model, introducing a new uniform-sampling technique for the degenerate ground states in this case that allows us to provide an unbiased estimate of the domain-wall fractal dimension. Finally, Sec. V discusses the compatibility of our results with the conjecture $d_{\text{f}} = 1 + 3/[4(3 + \theta)]$ of Ref. [38] and contains our conclusions.

II. MODEL AND ALGORITHMS

A. The model

We consider the random-exchange, zero-field Ising model with Hamiltonian

$$\mathcal{H} = -\sum_{\langle i,j \rangle} J_{ij} s_i s_j. \tag{1}$$

Here, $\langle i,j \rangle$ denotes summation over pairs of nearest neighbors. For the purposes of this study, the underlying lattice is chosen to have square elementary plaquettes, but the techniques described here are applicable *mutatis mutandis* to any regular planar graph (see, for instance, Refs. [42,56]). The case of nonplanar graphs is discussed in Sec. II C below.

The couplings J_{ij} are quenched random variables. At zero temperature, two distinct types of behavior are expected, one

for discrete and commensurate allowed coupling values and a second class for distributions with incommensurate or continuous support [15,17–19,57]. We consider one representative of each class, namely, the symmetric bimodal ($\pm J$) distribution,

$$P(J_{ij}) = \tfrac{1}{2}\delta(J_{ij} - J) + \tfrac{1}{2}\delta(J_{ij} + J), \qquad (2)$$

for the commensurate class and the symmetric Gaussian,

$$J_{ij} \sim \mathcal{N}(0,1), \qquad (3)$$

as example of the continuous class of distributions.

B. Matching with Kasteleyn cities

It was initially noted by Toulouse that the model (1) could be dualized and the trivial up-down symmetry of the states removed by considering the interactions around an elementary plaquette [58]. Each plaquette with an odd number of antiferromagnetic bonds is inherently *frustrated*, such that in each spin configuration at least one of the elementary interactions around the plaquette will be unsatisfied. The energy of the ground state of such a system will hence be elevated above the ground-state energy of a ferromagnet by an amount proportional to the total weight of such *broken* bonds. If edges of the *dual* lattice are used to indicate the broken bonds, these link together to form defect lines on the dual lattice, emanating and ending in frustrated plaquettes [23]. The search for a ground state is thus (for a planar lattice) equivalent to the determination of a *minimum-weight perfect matching* (MWPM) on the complete graph of frustrated plaquettes, where the edge weights correspond to the shortest paths (on the dual lattice) between each pair of frustrated plaquettes. For details see, e.g., Refs. [23,42]. As MWPM is a polynomial problem which is solved efficiently using the so-called blossom algorithm [59], it was first noted by Bieche *et al.* [23] that this allows to calculate exact ground states for relatively large systems.

In practice, however, the outlined mapping has certain disadvantages. The weighted distance between each pair of frustrated plaquettes needs to be determined before the matching can proceed. Since each plaquette could be matched up with any other, a solution is sought for the *complete* graph of frustrated plaquettes. The average number of such plaquettes is $F = \alpha N$, where N is the number of spins and α is a disorder-dependent constant that equals $\alpha = 1/2$ for the symmetric distributions considered here. The number of edges, however, is $F(F-1)/2$, increasing quadratically in the system volume. The original implementation of the blossom algorithm has complexity $O(V^2 E)$, where V is the number of vertices in the auxiliary graph and E the number of edges [59]. For the present problem, this corresponds to $O(L^8)$ scaling. Memory requirements are $O(L^4)$. While a number of algorithms with improved worst-case complexity have been proposed, not all of them are fast and hence useful in practice. We use here the currently fastest publicly available algorithm due to Kolmogorov [46]. As it is unlikely that edges with a very large weight are part of the minimum-weight matching, in practice only edges up to a certain weight are retained [23]. One has to proceed carefully here, however, to ensure high success rates also for larger system sizes. Strictly speaking, the resulting algorithm is merely quasiexact.

A polynomial-time solution to the Ising spin-glass ground-state problem on planar graphs based on a somewhat different mapping was proposed in Refs. [44,45]. This is a rather direct implementation of the interpretation of the Ising ground-state search as a maximum/minimum-cut problem. Splitting the Hamiltonian (1) into three terms as follows,

$$-\mathcal{H} = W^+ + W^- - W^\pm = K - 2W^\pm, \qquad (4)$$

where $K = \sum_{\langle ij \rangle} J_{ij}$ and

$$W^+ = \sum_{\substack{\langle ij \rangle \\ s_i = s_j = +1}} J_{ij}, \quad W^- = \sum_{\substack{\langle ij \rangle \\ s_i = s_j = -1}} J_{ij},$$

$$W^\pm = \sum_{\substack{\langle ij \rangle \\ s_i \neq s_j}} J_{ij}, \qquad (5)$$

it is clear that the energy is minimized for a configuration that minimizes $W^\pm$, which is the weight of the *cut* or, in more physical terms the interface, separating up spins from down spins. Note that the interface can consist of more than one connected components. As it turns out, such cuts can be related one-to-one to perfect matchings in an auxiliary graph. To see this, consider the example shown in Fig. 1. The right panel shows a configuration of up and down spins on a patch of the square lattice with free boundaries together with the corresponding cut of antialigned neighboring spins. The cut forms a set of closed loops on the dual lattice (red lines). To represent it as a matching, consider the auxiliary graph shown on the left of Fig. 1 that replaces each plaquette of the original lattice (i.e., each node of the dual lattice) by a complete graph of four nodes, a "Kasteleyn city." To create a regular lattice graph, the single outer plaquette of the dual graph is replaced by $4L$ individual plaquettes surrounding the original lattice. The cut on the right can then be represented as a perfect matching on the auxiliary graph as is shown in the middle panel of Fig. 1. Here, vertices that do not have cut lines adjacent to them will have all four vertices of the associated Kasteleyn city matched by the internal edges, such that after contracting back the Kasteleyn cities to regular vertices one ends up with the graph shown on the right, which represents the cut in spin language. To ensure that a MWPM corresponds to a minimum cut, we assign edge weights in the auxiliary graph that are equal to the coupling J_{ij} of the bond in the original graph that is crossed by the bond in the auxiliary graph. For bonds in the auxiliary graph that do not correspond to edges in the original graph, in particular the internal bonds of Kasteleyn cities as well as bonds between the additional external plaquettes, the weight is set to zero. Finally, a spin configuration consistent with the loops on the dual graph found in this way is constructed by flipping the spin orientation each time a loop line is crossed [44,45].

As the auxiliary graph used here has only $4(L+1)^2$ vertices and $6(L+1)^2 + 2L(L-1) = 8L^2 + 10L + 6$ edges (for periodic-free boundaries) as compared to the $O(L^2)$ vertices and $O(L^4)$ edges of Bieche's approach [23], it is significantly more efficient and, due to the smaller storage requirements, this approach allows to treat much larger systems sizes. In practice, we use the Blossom V implementation introduced in Ref. [46] to perform the MWPM calculations. The method can be easily generalized to other planar graphs,
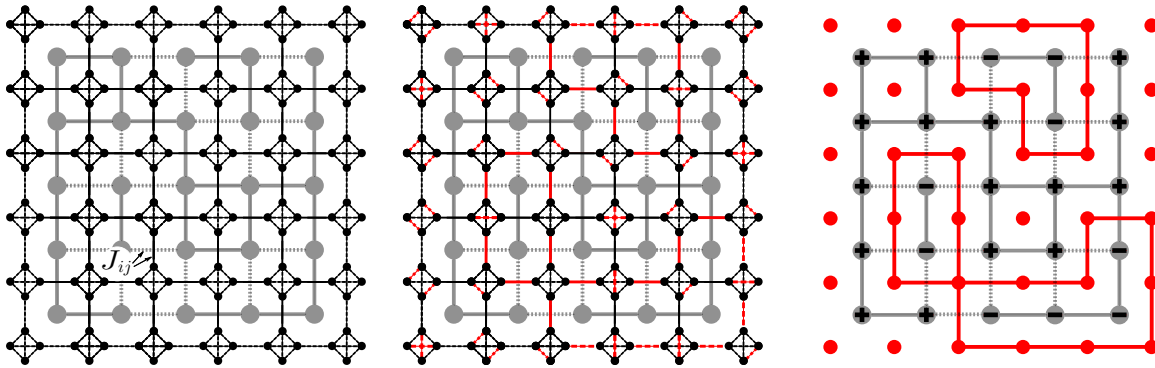
FIG. 1. Mapping of the Ising spin-glass ground-state problem to a minimum-weight perfect matching. An auxiliary graph is constructed by expanding each plaquette of the dual lattice into a complete graph K_4 of nodes (left). Additional rows and columns of K_4 nodes are added instead of the outer plaquette to make the auxiliary graph more regular. Edge weights on the auxiliary graph are J_{ij} for each bond that crosses a bond (i, j) of the original graph and zero otherwise. Then, a minimum-weight perfect matching is determined on the auxiliary graph (middle). By contracting the K_4 vertices again, the matching reduces to a minimum cut on the spin lattice, i.e., a set of closed loops surrounding islands of down spins in a sea of up spins or vice versa (right). Dashed bonds on the spin lattice correspond to antiferromagnetic couplings $J_{ij} < 0$, solid bonds to ferromagnetic ones, $J_{ij} > 0$.

for instance $L \times L$ graphs with periodic boundaries in one direction. In this case, the two additional lines of external plaquettes in either the horizontal or vertical direction can be removed, otherwise the algorithm proceeds in the same way. A generalization to nonplanar graphs is not possible, however, as then the one-to-one mapping between solutions of the MWPM problem and ground states of the spin system breaks down [45]: if the solution to the MWPM leads to loops that wrap around the lattice it is possible to find an odd number of loop lines in a given row or column of the lattice. In this case, it is not possible to find a spin configuration that is consistent with the lines.

C. Windowing technique for toroidal systems

Such a configuration with an odd number of line segments in a given row or column of an $L \times L$ system with fully periodic boundaries can be repaired by changing the boundary conditions in the corresponding direction from periodic to antiperiodic, corresponding to an extra loop wrapping around the lattice, thus resulting in an even number of lines again. In this sense, as discussed in Ref. [45], the approach outlined above finds an *extended ground state* for a system where the boundary conditions are added to the dynamical degrees of freedom. While this can be quite useful, it is not immediately applicable to the calculation of defect energies and domain walls, where specific, fixed boundary conditions need to be applied.

Nevertheless, a method for finding ground states for a fixed choice of periodic boundary conditions can be constructed from the MWPM approach outlined above, as we will now show. To achieve this, we successively determine exact ground states in square windows of size $L' \times L'$ ($L' < L$) with free boundary conditions, while the spin configuration outside of the window remains unchanged. By moving this window randomly over the full $L \times L$ lattice, the exact ground state is typically found after a moderate number of iterations. The sequence is started by initializing the system in a random spin configuration $\{s_i\}$. The origin of the window is then chosen randomly at one of the lattice sites, and the exact ground state of the spins inside of the window is determined using

MWPM, subject to the additional constraint of a layer of fixed spins surrounding it. These spins are fixed by placing very strong bonds with couplings J_{strong} between them that cannot be broken in the solution of the MWPM, for instance by choosing $|J_{\text{strong}}| > \sum_{\langle ij \rangle} |J_{ij}|$. We choose $J_{ij} = +|J_{\text{strong}}|$ for parallel spins along the boundary of the window and $J_{ij} = -|J_{\text{strong}}|$ for antiparallel ones to ensure that these spins do not change their relative orientation as a result of the MWPM run. This setup is illustrated in Fig. 2.

As the spins at window boundaries are fixed and the resulting constraint optimization problem is solved exactly, each iteration of the windowing method decreases the energy of the total system or leaves it invariant. We observe convergence of the method after a moderate number n of iterations. The process is illustrated in Fig. 3, where we display the overlap $s_i s_i^0$ with the exact ground state s_i^0 for an example disorder configuration of linear size $L = 200$ with Gaussian couplings starting from a random initial spin configuration. It is seen how even the first optimization with a window of size $L' = L - 2 = 198$ leaves only a single (large) cluster excitation over the ground state. As is seen from the following panels, such excitations can only be fully relaxed if the window does not intersect them. Hence the time until convergence is a random variable. To determine a good set of parameters we performed test runs for different sizes L and L' of the system and the window, respectively, and with a varying number of iterations. The results show that the necessary number of iterations depends both on L' and the initial spin configuration, such that larger L' needs smaller n, and if the initial spin configuration is changed, n will also change. As is intuitively plausible, we find best results for the largest windows, and so we fixed the window size to its maximum $L' = L - 2$ for all runs. To decide whether a given run arrives in one of the ground states, we compared against exact results for system sizes $L \leqslant 100$ produced by the branch-and-cut method implemented in the spin-glass server [60]. For larger system sizes, we used the lowest energy found in a sequence of independent runs as an estimate of the ground-state energy and measured the success probability $P_n(\{J_{ij}\})$ as the proportion of runs that ended in
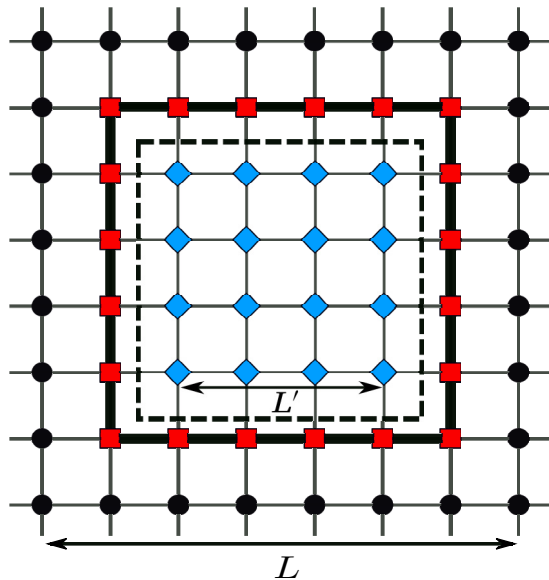
FIG. 2. Schematic representation of the windowing technique to determine ground states for toroidal systems. The dashed square shows the window and the blue diamonds represent the sites whose spins will be updated next by the windowing technique, as they are contained within the current window. Red squares indicate sites whose spins are fixed in their current orientation with strong bonds, indicated by the thick black lines. As a result, the MWPM problem will be solved for the system of red and blue spins with using free boundary conditions.

this lowest-energy state found or in the exact ground-state for the system sizes treated by the spin-glass server. The resulting success probability data, estimated from between 250 ($L \geqslant 700$) to 2000 ($L \leqslant 150$) runs for different initial

spin configurations for each disorder realization, is collected in Table II. As is clearly seen, the success probabilities are rather high such that for $n = 20$, for instance, they are consistently above 70%. There is almost no size dependence of the average success probability $\overline{P}_n$, so the hardness of finding ground states for the fully periodic torus lattices with the proposed method does not increase with system size.

Still, from the data presented in Table II, it is clear that not every run of the windowing method converges to the ground state. To further increase the success probability of the method, we use repeated runs and pick the lowest energy found there [61]. If the success probability for a given sample in runs of n iterations is $P_n(\{J_{ij}\})$, then the probability of finding the ground state at least once in m independent runs is

$$P_s(\{J_{ij}\}) = 1 - [1 - P_n(\{J_{ij}\})]^m, \qquad (6)$$

and this can be tuned arbitrarily close to unity by increasing m. If we set a desired success probability of, say, $P_s = 0.999$, we can use Eq. (6) to determine the required number m of repetitions. For each realization we hence find

$$m(\{J_{ij}\}) = \ln[1 - P_s] / \ln[1 - P_n(\{J_{ij}\})].$$

In Table III, we show the values of $\overline{m}$ averaged over 100 disorder realizations as a function of L and n. Clearly, the dependence on system size is weak. The total computational effort of such repeated runs is proportional to $m \times n$. From the values of n tested in Table III, this effort is found to be minimal for $n = 10$, and we use $m = 8$ repetitions independent of system size to find the exact ground state in approximately 99.9% of the samples. As an additional protection against potential outliers we demand that the lowest-energy state found in these $m = 8$ runs must have occurred at least three out of these eight times. If this is not the case, another eight runs are performed etc. This adds only a tiny fraction of extra average
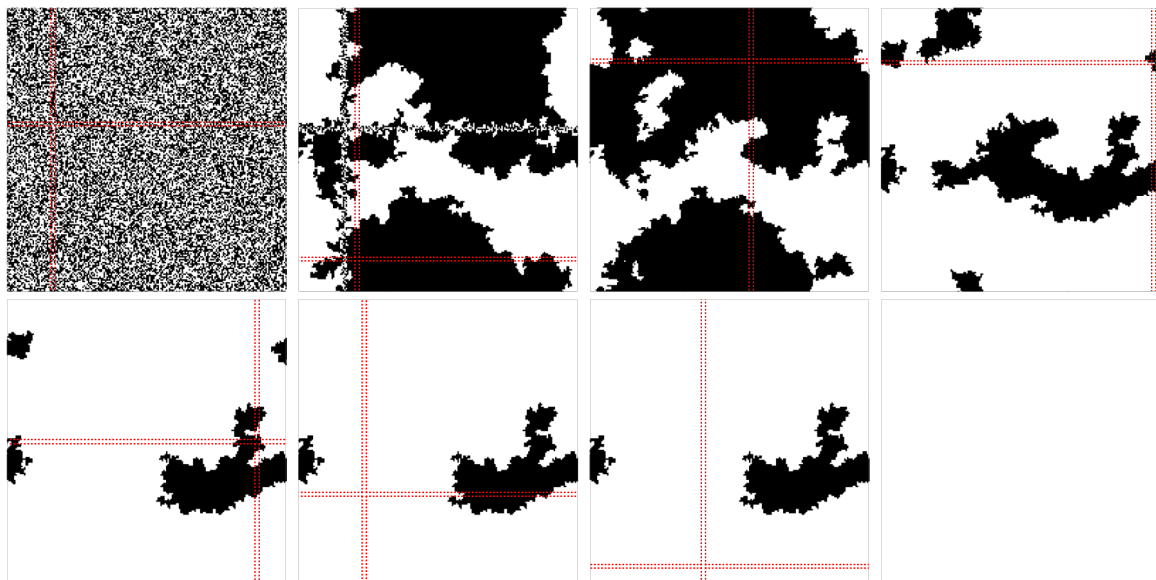

FIG. 3. Application of the windowing method to find a ground state of a sample with toroidal boundaries. Spins on white lattice sites are consistent with the ground-state orientation s_i^0, i.e., $s_i s_i^0 = +1$, black spins are oppositely oriented, i.e., $s_i s_i^0 = -1$. In a random initial configuration, the spins have $s_i s_i^0 = \pm 1$ uniformly at random (top left). Exact ground states are found in windows of size $(L - 2) \times (L - 2)$ placed at a random location (red dotted lines), with the remaining spins acting as fixed boundaries. After a few iterations, all spins have the ground-state orientation (bottom right).

TABLE II. The average probability $\overline{P}_n$ of finding the ground state (success probability) for $20 \leqslant L \leqslant 1000$, and for different numbers n of iterations. Results are averaged over 100 disorder realizations.

$L \backslash n$	5	10	15	20	25	30
20	0.276	0.561	0.671	0.728	0.762	0.782
50	0.317	0.603	0.705	0.756	0.790	0.805
80	0.315	0.592	0.700	0.752	0.783	0.806
100	0.315	0.594	0.700	0.745	0.779	0.789
150	0.326	0.611	0.714	0.768	0.797	0.821
200	0.323	0.610	0.712	0.765	0.792	0.814
350	0.340	0.628	0.729	0.789	0.822	0.833
500	0.317	0.589	0.683	0.740	0.771	0.801
700	0.329	0.612	0.723	0.770	0.782	0.818
1000	0.322	0.609	0.713	0.764	0.779	0.807

runtime, but it will be able to catch a few of the 0.01% of samples where the ground state would otherwise not be found. As a test, we applied this combined technique to the samples for $L \leqslant 100$ where the exact ground-state energy is known and it arrived in a ground state in all cases.

D. Performance of the algorithm

It is interesting to see how the matching based on Kasteleyn cities for planar instances as well as the windowing method outlined above for toroidal graphs fare in computational efficiency as compared to the more general approaches implemented in the spin-glass server [60]. The run times in seconds on standard hardware are shown for periodic-free boundary conditions (PFBC) and for periodic-periodic (toroidal) boundaries (PPBC) as compared to the corresponding results of the spin-glass server for system sizes $L \leqslant 100$ in Table IV. For PFBC, the matching approach is always much faster than the method used by the spin-glass server, which is based on a modified exact numeration technique known as branch-and-cut. For PPBC, the windowing technique introduces a certain overhead, such that a crossover is observed with branch-and-cut being faster for $L \lesssim 20$ and the windowing method winning out for $L \gtrsim 20$.

TABLE III. The average number $\overline{m}$ of repetitions required according to Eq. (6) for runs of the windowing technique with n random placements of the window per run to ensure an overall success probably of $P_s = 0.999$.

$L \backslash n$	5	10	15	20	25	30
20	23.5	9.3	6.9	5.8	5.3	4.9
50	19.7	8.2	6.2	5.3	4.7	4.5
80	20.2	8.6	6.4	5.4	4.9	4.4
100	20.0	8.5	6.4	5.6	4.9	4.5
150	19.2	8.1	6.0	5.0	4.5	4.0
200	19.2	8.3	6.1	5.3	4.7	3.6
350	18.4	7.4	5.8	4.8	3.9	3.8
500	21.2	8.5	7.0	6.0	5.0	4.6
700	20.3	7.9	6.3	5.8	4.6	5.0
1000	20.0	8.5	6.4	5.1	5.0	4.5

TABLE IV. Average run time (in seconds) for determining a ground state of samples with periodic-free boundaries (PFBC) and periodic-periodic boundaries (PPBC), respectively, using the minimum-weight perfect matching (MWPM) approach based on Kasteleyn cities for PFBC and the windowing technique (WT) for PPBC as compared to the times reported by the spin-glass server (SGS) on the same samples.

L	PFBC		PPBC	
	SGS	MWPM	SGS	WT
8	0.00228	0.000203	0.00560	0.02468
10	0.01330	0.000424	0.01950	0.04462
20	0.18330	0.002361	0.22820	0.19119
50	3.38740	0.024184	3.93040	2.18788
80	31.0738	0.069104	35.7004	6.42005
100	150.218	0.115761	189.501	9.81247

The scaling of run times with system size is illustrated in Fig. 4. The algorithm of the spin-glass server utilized here is based on branch-and-cut [62], which corresponds to a combination of a cutting plane technique with the iterative removal of branches of the search tree that cannot contain a solution. While this approach is quite efficient, and outperforms other exact methods for hard problems, its run-time still scales exponentially with system size. The super-polynomial behavior is clearly seen in the doubly logarithmic representation of Fig. 4. For the matching approach for PFBC, the implementation used here has $O(L^6)$ worst-case scaling [46]. As the straight line indicates, we indeed see clear power-law behavior, but the average run times probed here increase much more gently with system size. A power-law fit of the form

$$t(L) = A_t L^\kappa \tag{7}$$

to the data yields $\kappa = 2.22(2)$, so the scaling is only slightly worse than linear in the volume in the considered range of system sizes.
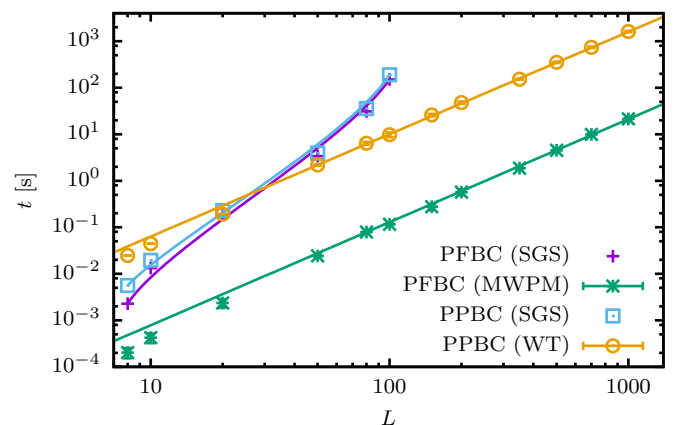

FIG. 4. Average time t per sample to determine ground states of systems with PFBC and PPBC for $L \times L$ samples using the minimum-weight perfect matching (MWPM) method for periodic-free samples (PFBC), the windowing technique (WT) for periodic-periodic samples (PPBC), and the spin-glass server (SGS), respectively. The straight lines are fits of the form (7) to the data, whereas the lines for the SGS data are just interpolations to guide the eye.

Finally, for the windowing technique built on top of MWPM for the PPBC samples, we find an overhead that is to a very good approximation independent of system size, such that calculations for PPBC are by a factor of 80 more expensive that those for samples with PFBC for the chosen confidence level of $P_s = 0.999$, corresponding to the $n = 10$ iterations and $m = 8$ repetitions. A fit of the form (7) to the data for PPBC yields $\kappa = 2.20(2)$, perfectly consistent with the results for PFBC. The ratio of amplitudes A_t is estimated as $A_t = 83 \pm 12$, consistent with the expected value of slightly above 80 resulting from the additional requirement of a threefold occurrence of the ground state.

III. RESULTS FOR GAUSSIAN COUPLINGS

For the Gaussian distribution (3) the set of couplings for which exact degeneracies occur is expected to be of zero measure. The present techniques based on matching hence directly yield the correct distribution of states at zero temperature.

A. Ground-state energies

The average ground-state energy per spin, $\langle e(L) \rangle_J$, depends on the coupling distribution. Additionally, we expect finite-size corrections which in turn are sensitive to the boundary conditions employed [55,63,64]. Following Ref. [55], one expects a Wegner correction exponent $\omega(d) = (6 - d) + \cdots$ to leading order, whereas numerically one finds [9] $\omega \approx 1.0$ for Ising spin glasses in $d = 3$ and $\omega \approx 0.75$ for $d = 2$ [11]. As then $-(d - \theta) + \omega \approx -3.03$ in two dimensions, this implies that nonanalytic corrections are substantially suppressed against the leading analytic ones in this quantity. We hence assume the following general form for the size dependence of the average ground-state energy:

$$\langle e(L) \rangle_J = e_\infty + A_E L^{-(d-\theta)} + C_E L^{-1} + D_E L^{-2} + E_E L^{-3} + \dots . \tag{8}$$

The presence of a term proportional to $L^{-(d-\theta)}$ follows from standard arguments about the scaling of the correlation length and the free-energy density [65], taking additionally into account that for a $T = 0$ critical point the $1/\beta^2$ prefactor in the relation $e = (-1/\beta^2)\mathrm{d}(\beta f)/\mathrm{d}T$ is critical, as well as making use of the relation $\nu = -1/\theta$ [55]. Although this derivation should apply for any $T = 0$ critical point, for the spin glass it is tempting to attribute the occurrence of the $L^{d-\theta}$ term to the presence of domain-wall defects that are trapped in the system due to periodic boundary conditions. In Ref. [55], it is suggested to reduce the number of parameters in Eq. (8) by considering the energy $\hat{e}(L)$ per bond instead of the energy $e(L)$ per site. If one assumes that depending on the boundary conditions this quantity has a $1/L$ correction for any free edge and a $1/L^2$ correction for any corner, for the square lattice with its two bonds per site we expect

$$2\langle \hat{e}(L) \rangle_J = e_\infty + \hat{A}_E L^{-(d-\theta)} + \hat{C}_E L^{-1} + \hat{D}_E L^{-2}$$

up to higher-order corrections. For free-free boundaries, one has $E(L) = L^2 e(L) = (2L^2 - 2L)\hat{e}(L)$ and hence

$$\langle e(L) \rangle_J = e_\infty + \hat{A}_E L^{-(d-\theta)} + (\hat{C}_E - e_\infty)L^{-1} + (\hat{D}_E - \hat{C}_E)L^{-2} - \hat{D}_E L^{-3}, \tag{9}$$

where a term of order $L^{-(d-\theta)-1}$, which for $\theta < 0$ is asymptotically smaller than $1/L^3$ has been neglected. This is of the form of Eq. (8), but with the $1/L^3$ term merely being produced by the $1/L^2$ correction in $\hat{e}(L)$, such that there are only five fit parameters in (9) as compared to six parameters in Eq. (8). For periodic-free boundaries there is a free edge but no corners, such that $\hat{D}_E = 0$ and $E(L) = (2L^2 - L)\hat{e}(L) = L^2 e(L)$, and we find

$$\langle e(L) \rangle_J = e_\infty + \hat{A}_E L^{-(d-\theta)} + (\hat{C}_E - e_\infty/2)L^{-1} - (\hat{C}_E/2)L^{-2}, \tag{10}$$

where again a term proportional to $L^{-(d-\theta)-1}$ was omitted. For periodic-periodic boundaries, on the other hand, one should have $\hat{C}_E = 0 = \hat{D}_E$, and hence only a correction proportional to $L^{-(d-\theta)}$. We will test the validity of these assumptions for our data below.

Beyond the mean ground-state energy, it is interesting to study the shape of the energy distribution over different disorder samples. It has been shown in Ref. [63], based on results of Wehr and Aizenman [66], that the width of this distribution scales as L^{Θ_f} with $\Theta_f = -d/2$. Below, we investigate the distribution shape by direct inspection and by analyzing the scaling of its kurtosis defined by

$$\mathrm{Kurt}[e] = \frac{\langle (e - \langle e \rangle_J)^4 \rangle_J}{[\langle (e - \langle e \rangle_J)^2 \rangle_J]^2} \tag{11}$$

with system size, where $\mathrm{Kurt}[\cdot] = 3$ for a Gaussian distribution.

B. Domain-wall calculations

The analysis of defect energies provides a convenient way of studying the stability of the ordered phase. In the most common approach, one inserts system-spanning domain walls into the system by a suitable change of boundary conditions [67]. The energy of such excitations scales as a power of their linear size [50],

$$E_{\mathrm{def}} \propto L^\theta, \tag{12}$$

where the spin-stiffness exponent θ depends on the symmetries of the model as well as the lattice dimension d. In a simple generalization of Peierls' argument for the stability of the ferromagnetic phase, one concludes that a spin-glass phase is stable against thermal fluctuations up to some $T_c > 0$ if $\theta > 0$ and unstable for $\theta < 0$, with $\theta = 0$ denoting the marginal case. The conceptually most direct way of inserting a domain-wall excitation is to compute a ground-state for free boundaries in, say, the x direction as a reference and to then fix the boundary spins along the x boundary in opposite relative orientations as compared to this state for a second ground-state calculation. The excess energy in the second run corresponds to the energy contained in the domain wall. This setup is sometimes referred to as domain-wall boundary condition [14,54]. An alternative proposed initially by Banavar [67] uses the difference between the ground-state energies for periodic and for antiperiodic boundaries in x direction. The resulting value of $\Delta E = E_{\mathrm{P}} - E_{\mathrm{AP}}$ is potentially the difference of energies of two configurations with such domain walls as the periodicity of both P and AP boundaries can force a domain wall into the system [68,69],

but this difference is found to nevertheless scale with the same stiffness exponent as for domain-wall boundaries [54].

For calculations based on MWPM alone one needs to apply free boundaries in y direction in order to ensure planarity of the lattice. With the help of the windowing technique it is also possible to implement this procedure for samples with periodic-periodic boundaries, however. In general we expect the leading scaling to be accompanied by scaling corrections of the form [64]

$$\langle |\Delta E(L)| \rangle_J(L) = A_\theta L^\theta (1 + B_\theta L^{-\omega}) + \frac{C_\theta}{L} + \frac{D_\theta}{L^2} + \cdots,$$
(13)

where ω denotes the leading corrections-to-scaling exponent, and $1/L$ and $1/L^2$ are analytic corrections [65]. For the setup with domain-wall boundary conditions significantly stronger, corrections have been observed than for the P-AP situation [54] and we hence concentrate on the latter approach here.

Apart from the energy density of domain walls or droplet boundaries another contentious question is that of the geometric nature of excitations in spin glasses. While it is not ultimately clear whether droplets or domain walls are the fundamental objects in this system or rather some more esoteric form of excitations such as sponges exist [70–72], it is interesting to see whether domain walls are stochastically fractal objects and if the corresponding fractal dimension $d_f < d$ or rather domain walls can be space filling [73]. We determined the domain wall as the set $\mathcal{D}$ of all dual bonds for which

$$[J_{ij}s_is_j]^{(\text{P})}[J_{ij}s_is_j]^{(\text{AP})} < 0.$$
(14)

The inclusion of the couplings J_{ij} in the product takes care of the fact that across the edge where the boundary condition is changed from P to AP the spins will be in different relative orientation before and after the change, but this is merely a consequence of the flip $J_{ij} \rightarrow -J_{ij}$ of the couplings there and should not be counted as a part of the induced domain wall. We denote by ℓ the number of (dual) edges in the set $\mathcal{D}$. Following the usual box-counting argument, scaling according to $\langle \ell \rangle_J \sim L^{d_f}$ defines the domain-wall fractal dimension d_f. As for the defect energies we anticipate the presence of corrections, leading to the scaling form

$$\langle \ell \rangle_J(L) = A_\ell L^{d_f}(1 + B_\ell L^{-\omega}) + \frac{C_\ell}{L} + \frac{D_\ell}{L^2} + \cdots.$$
(15)

C. Periodic-free boundaries

For the periodic-free setup (PFBC) we used the MWPM approach for periodic and antiperiodic boundaries in x direction and system sizes ranging from $L = 8$ up to $L = 10\,000$. For $L \leqslant 350$ we generated 10^6 disorder configurations, while for larger systems the number of replicas is gradually reduced down to about 300 for $L = 10\,000$, see the details collected in Table V. We used the MIXMAX random number generator [74,75], which has provably good statistical properties and also passes all of the tests in the suite TESTU01 [76]. As an additional check in view of the high-precision nature of the present study, part of our calculations were repeated with Mersenne twister [77]. All results were found to be perfectly consistent within error bars.

TABLE V. The number of disorder realizations for different boundary conditions, coupling distributions and system sizes.

L	PFBC Gaussian	PPBC Gaussian	PFBC bimodal
8	1×10^6	1×10^5	1×10^5
10	1×10^6	1×10^5	1×10^5
20	1×10^6	1×10^5	1×10^5
30	1×10^6	1×10^5	1×10^5
40	1×10^6	1×10^5	1×10^5
50	1×10^6	1×10^5	1×10^5
80	1×10^6	8×10^4	1×10^5
100	1×10^6	8×10^4	1×10^5
150	1×10^6	1×10^5	1×10^5
200	1×10^6	5×10^4	8×10^4
350	5×10^5	5×10^4	8×10^4
500	5×10^5	3×10^4	5×10^4
700	5×10^5	1×10^4	3×10^4
1000	3×10^5	1×10^4	1×10^4
1500	1×10^5	7×10^3	5×10^3
2000	5×10^4	1×10^3	3×10^3
3000	3×10^4	640	1505
4000	2×10^4		
5000	3×10^3		
7000	400		
8000	455		
10000	265		

We start by considering the ground-state energies. Here, we use the results for both P and AP boundary conditions. They differ from each other, on average, by far less than the statistical errors would suggest, but this is due to the fact that for each sample both energies are highly correlated. For studying the average ground-state energy, we hence calculated the average $\bar{E} = (E_\text{P} + E_\text{AP})/2$ and estimated statistical errors for $\langle \bar{E} \rangle_J$ through the variation over disorder samples. As the data in panel (a) of Fig. 5 show, the finite-size corrections to scaling are relatively small, with the result for $L = 10$ only being about 4% above the asymptotic value. Due to the large range of system sizes and high statistics in disorder samples we get a stable result for the full nonlinear five parameter fit of the form (10) to the data with a quality of fit[1] of $Q = 0.81$. For the asymptotic ground-state energy, we find

$$e_\infty = -1.314\,787\,6(7),$$

while the spin-stiffness exponent $\theta = -0.273(65)$ from this fit.[2] If we fix θ at the value $\theta = -0.2793$ found below from the defect energy calculations for the PFBC boundaries, the

---

[1]Q is the probability that a χ^2 as poor as the one observed could have occurred by chance, i.e., through random fluctuations, although the model is correct [92].

[2]Note that hence the form (10) is found to describe the data perfectly well, in contrast to the corresponding form used in Ref. [55], cf. Eq. (22) there, which is not consistent with the equation derived here. We also attempted a more general fit with unrestricted amplitudes for the $1/L$ and $1/L^2$ terms and found the resulting estimate of e_∞ as well as the amplitudes to be consistent with the fit discussed in the main text.
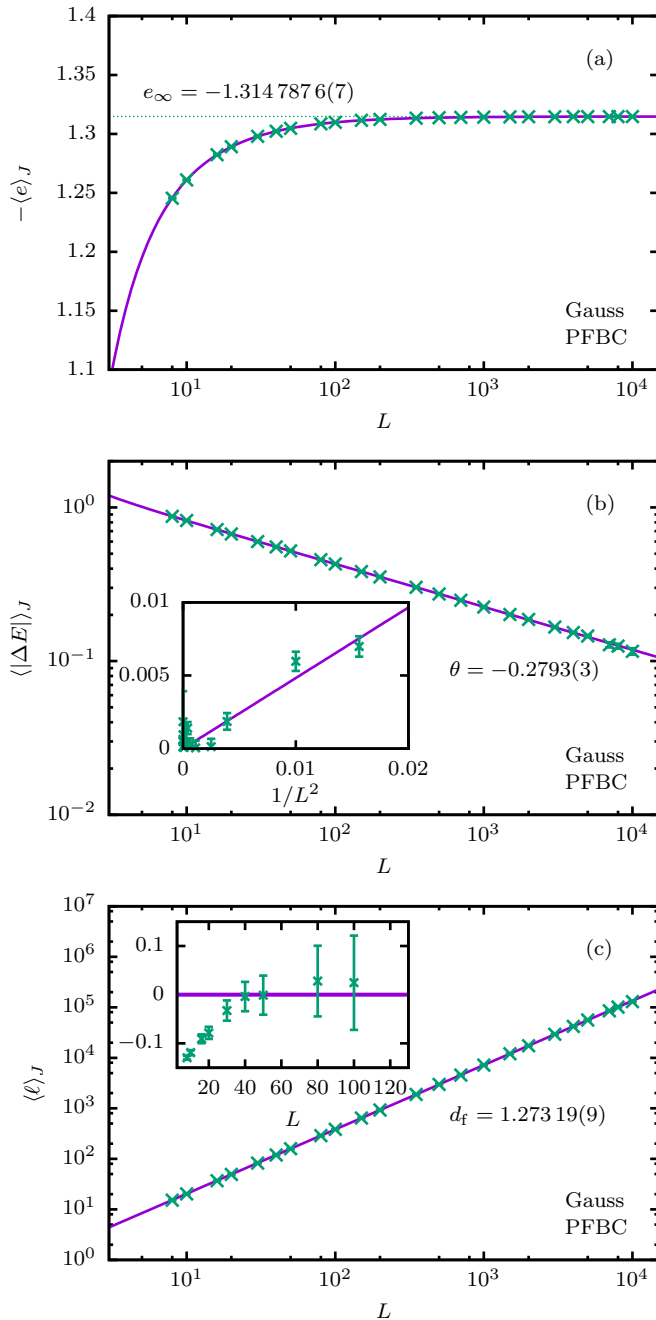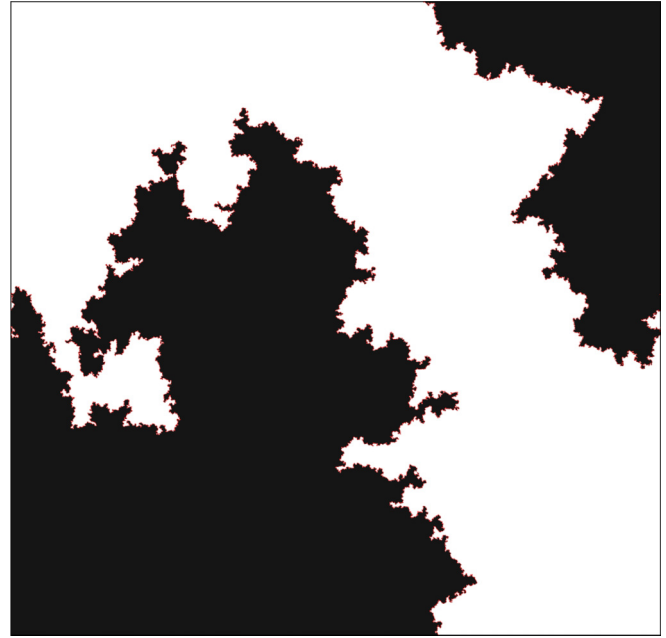
FIG. 6. Overlap configuration of the ground states for P and AP boundaries for a $L = 10\,000$ disorder realization of the PFBC Gaussian system. The red line demarcates the domain wall which traverses $\ell = 233\,141$ dual links.

asymptotic ground-state estimate e_∞ is unaltered from the above value up to the given number of digits. On gradually increasing $L_{\min}$ we find statistically consistent fits that, however, become less and less stable as the number of degrees of freedom is reduced. The resulting estimate of e_∞ is unaltered within statistical errors.

Our data for the defect energies are shown in Fig. 5(b). We find scaling corrections to be small and a pure power-law fit without corrections yields a quality of fit $Q = 0.37$ for $L \geqslant L_{\min} = 50$. The corresponding estimate of the stiffness exponent is $\theta = -0.2798(4)$. Corrections can hence only be clearly resolved for $L \lesssim 50$. There, we find that the data are very well described by a single correction term proportional to $1/L^2$, cf. the inset of Fig. 5(b), where we show the residual contribution $\langle |\Delta E| \rangle_J - A_\theta L^\theta$ plotted against $1/L^2$. Our θ estimate from this fit is

$$\theta = -0.2793(3)$$

with $Q = 0.16$ when including all lattice sizes. Gradually increasing $L_{\min}$ does not reveal any discernible drift in the estimate for θ. Since we have one free boundary one might have expected the presence of a $1/L$ correction, which is clearly present in the ground-state energy itself according to the fit following Eq. (10). In the energy difference ΔE, however, this contribution cancels out since the couplings along the free edge are absent in both samples. If we nevertheless include such a term in the fit, its amplitude is found to be consistent with zero. We are not able to clearly resolve a Wegner correction $\propto L^{-\omega}$, which is not surprising since, as discussed above, we expect it to be clearly weaker than $1/L^2$.

We finally turn to the domain-wall length. Figure 6 shows a sample configuration with $L = 10\,000$ illustrating the meandering nature of the domain wall. For the average

FIG. 5. (a) Disorder-averaged ground-state energy per site $\langle e \rangle_J = \langle \bar{E}/L^2 \rangle_J$ for PFBC and Gaussian couplings together with a fit of the form (10) to the data in the range $L = 10, \ldots, 10\,000$. (b) Average defect energies $\langle |\Delta E| \rangle_J$ for the same system as calculated from the difference in ground-state energies between periodic and antiperiodic boundary conditions in the x direction. The points show our data for $8 \leqslant L \leqslant 10\,000$ and the solid line represents a fit of the form $\langle |\Delta E| \rangle_J(L) = A_\theta L^\theta + C_\theta/L^2$ to the data. The inset shows the correction $\langle |\Delta E| \rangle_J(L) - A_\theta L^\theta$ plotted against $1/L^2$ illustrating that this single term describes the corrections very well. (c) Average length ℓ of the domain-wall in the overlap of ground states for periodic and antiperiodic boundaries in x direction and free boundaries in y direction (PFBC boundaries). The line shows a fit of the functional form $\langle \ell \rangle_J = A_\ell L^{d_{\mathrm{f}}}$ to the data for $L \geqslant L_{\min} = 40$. The inset shows a blow-up of the deviations for small L.

domain-wall length, we find very clean scaling for PFBC as is seen from our data depicted in Fig. 5(c). A fit of the pure power-law form $\langle \ell \rangle_J = A_\ell L^{d_f}$ yields a fit quality of $Q = 0.56$ for $L_{\min} = 40$. The corresponding estimate of the fractal dimension is

$$d_f = 1.273\,19(9).$$

The deviations from a pure power law visible for system sizes $L < 20$ are rather small and not well described by a single correction term. We hence prefer to take them into account by simply omitting data from the small-L side instead of performing corrected fits. On systematically varying $L_{\min}$ in these fits, we find a drift only for $L_{\min} \leqslant 30$ and mutually consistent results for larger $L_{\min}$.

D. Periodic-periodic boundaries

For fully periodic or toroidal boundaries (PPBC), we use the windowing technique discussed above in Sec. II C to find exact ground states in more than 99.9% of the cases. Due to the increase in effort by the constant factor of 80 resulting from the windowing technique, we reduced the maximum system size a bit and considered lattices in the range $8 \leqslant L \leqslant 3000$. Additionally, the number of disorder realizations considered was reduced correspondingly, the exact numbers are shown in Table V.

Our data for the ground-state energies for PPBC are shown in Fig. 7(a), illustrating that finite-size corrections in this case are tiny, even much weaker than for the PFBC case. According to the discussion above, for the ground-state energies we do not expect the presence of analytic corrections for PPBC, and so we assume a scaling form

$$\langle e \rangle_J = e_\infty + A_E L^{-(2-\theta)}. \tag{16}$$

Fits of this form work very well and yield fit qualities of $Q > 0.4$ for all $L_{\min} \geqslant 10$. For $L_{\min} = 16$, we find

$$e_\infty = -1.314\,788(3)$$

as well as $\theta = -0.35(14)$ and $A = 1.51(65)$ with a good $Q = 0.60$. This fit is shown together with the data in panel (a) of Fig. 7.

For the defect energies, the data again show clear power-law scaling with L, see Fig. 7(b). For $L \geqslant L_{\min} = 50$, we get an excellent fit ($Q = 0.74$) for the pure power-law $\langle |\Delta E| \rangle_J = A_L L^\theta$ with $\theta = -0.2778(14)$. Regarding scaling corrections, it turns out that the size range where they are visible is rather small. As the inset of Fig. 7(b) shows, corrections are well described by a single $1/L^2$ term, consistent with the findings for the PFBC case. A corresponding fit for $L_{\min} = 10$ yields high quality with $Q = 0.92$ and

$$\theta = -0.2778(11).$$

A systematic trend on successively increasing $L_{\min}$ is not visible.

Regarding the domain-wall length, we again find only tiny scaling corrections, which cannot be resolved for any $L > 20$. To avoid any risk from spurious remnant corrections, we take $L_{\min} = 40$ for the uncorrected fit $\langle \ell \rangle_J = A_\ell L^{d_f}$ and arrive at
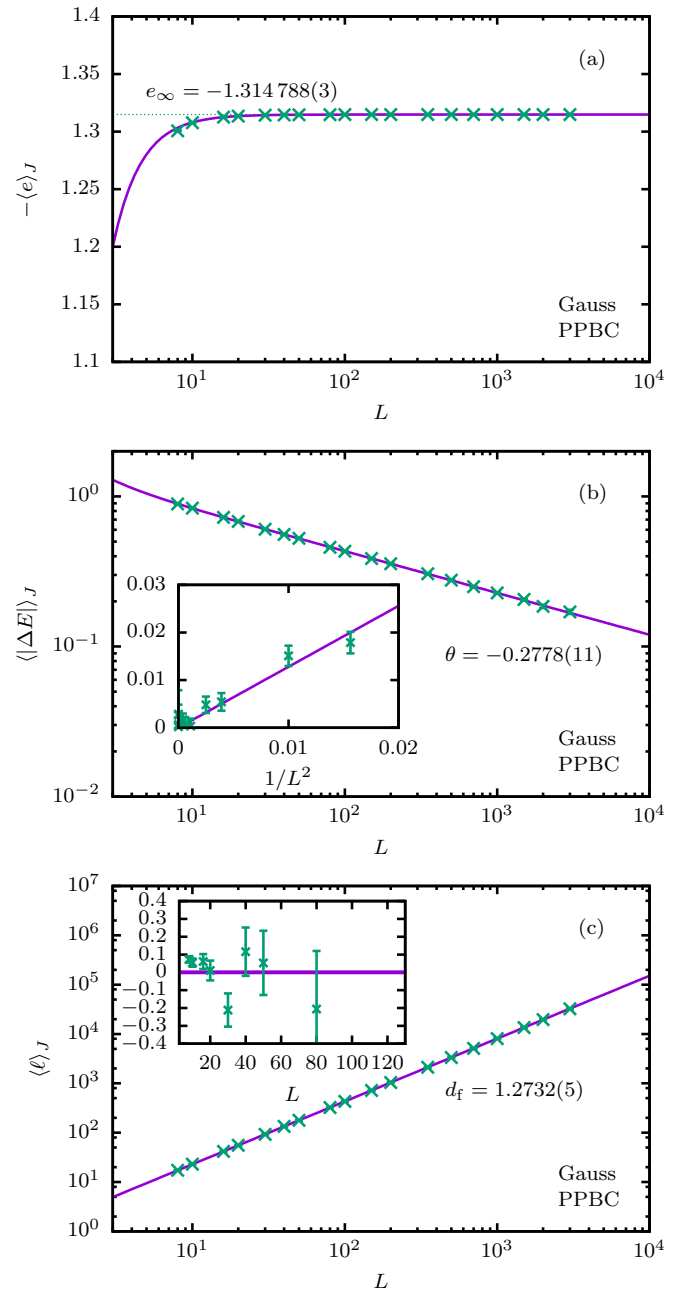
$$d_f = 1.2732(5),$$

FIG. 7. (a) Average ground-state energies for PPBC and Gaussian couplings together with a fit of the form (16) to the data in the range $L \geqslant L_{\min} = 16$. (b) Scaling of defect energies for the Gaussian model with fully periodic boundary conditions. The solid line shows a fit of the form $\langle |\Delta E| \rangle_J(L) = A_\theta L^\theta + C_\theta/L^2$ to the data. The inset shows the correction $\langle |\Delta E| \rangle_J(L) - A_\theta L^\theta$ plotted against $1/L^2$ illustrating that this single term describes the corrections very well. (c) Scaling of the length of the domain wall between P and AP ground states for the Gaussian PPBC case. The solid line shows a fit of the form $\langle \ell \rangle_J = A_\ell L^{d_f}$ to the data with $L_{\min} = 40$. The inset shows a detail of the main plot for small L.

which yields $Q = 0.73$. This fit is shown together with the data in Fig. 7(c). Comparing the results for θ and d_f between the PFBC and PPBC cases we see that they are in perfect agreement with each other, indicating that the results truly probe the

asymptotic regime and acting as an *ex post* verification of the correctness of the windowing technique for the PPBC case.

E. Probability distributions

When investigating the ground-state and defect energies as well as the domain-wall lengths, besides looking at the average values reported above it is also instructive to study the full distributions of these quantities over disorder samples. The width $\langle (e - \langle e \rangle_J)^2 \rangle_J$ of the distribution of ground-state energies per spin shows power-law scaling according to L^{Θ_f}, where we find $\Theta_f = -0.9995(3)$ for PFBC and $\Theta_f = -1.002(1)$ for PPBC, consistent with the theoretical expectation [63] $\Theta_f = -d/2$. The latter follows from a standard argument of decomposition of the system into effectively uncorrelated subsystems, such that the total energy is a sum of independent contributions. As a result, in the thermodynamic limit the distribution narrows to a delta peak, consistent with the fact that the ground-state energy is self-averaging [78]. To investigate the shape of the distribution, we studied its kurtosis defined in Eq. (11). Kurt[e] is shown in Fig. 8(a) for the PFBC case, where it is found to be consistent with 3 to within statistical errors for all lattice sizes $L \geqslant 20$, indicating that the distribution of ground-state energies is in fact Gaussian [79]. This is in contrast to systems with long-range interactions such as the Sherrington-Kirkpatrick model, where non-Gaussian distributions are found [63].

For symmetric coupling distributions the histogram of defect energies for P and AP boundaries is also symmetric and so has zero mean. It is expected that the standard deviation $\sigma(E)$ has the same asymptotic scaling behavior as the modulus $|\Delta E|$, and this is consistent with our observations. Considering the data for $\sigma(\Delta E)$ for PFBC, we use a pure power-law fit with $L \geqslant L_{min} = 30$ to find $\theta = -0.2793(3)$ ($Q = 0.55$). For PPBC, on the other hand, the same analysis yields $\theta = -0.279(2)$ and $Q = 0.81$ for the same range. In Fig. 8(b), we show the defect energy distribution for PFBC systems for a number of different lattice sizes, rescaled by the factor L^θ with $\theta = -0.2793$ describing the decay in width. As the Gaussian distribution with the same mean and width shows, the defect energy distribution is clearly not normal, but instead has much heavier tails.[3] This is confirmed by an inspection of the distribution kurtosis, Kurt[ΔE], which is found to be consistent with Kurt[ΔE] = 4.70(2) for systems of size $L \geqslant L_{min} = 20$.

The standard deviation of the distribution of domain-wall lengths is found to have the same scaling as the mean, i.e., it is asymptotically proportional to L^{d_f}, suggesting a complementary way of determining the fractal dimension. This approach yields estimates of $d_f = 1.2740(3)$ for PFBC ($L_{min} = 40$, $Q = 0.34$) and $d_f = 1.276(2)$ for PPBC ($L_{min} = 50$, $Q = 0.61$), respectively. The result for PFBC is slightly high as compared to the result from the mean, but still statistically consistent: the deviation is 2.6 times the combined error bar, but this does not take into account that the two error estimates are

---

[3]We note that there might be a relation between the behavior of the defect-energy distribution at vanishing energies and the question of a multiplicity of states in spin glasses [93].
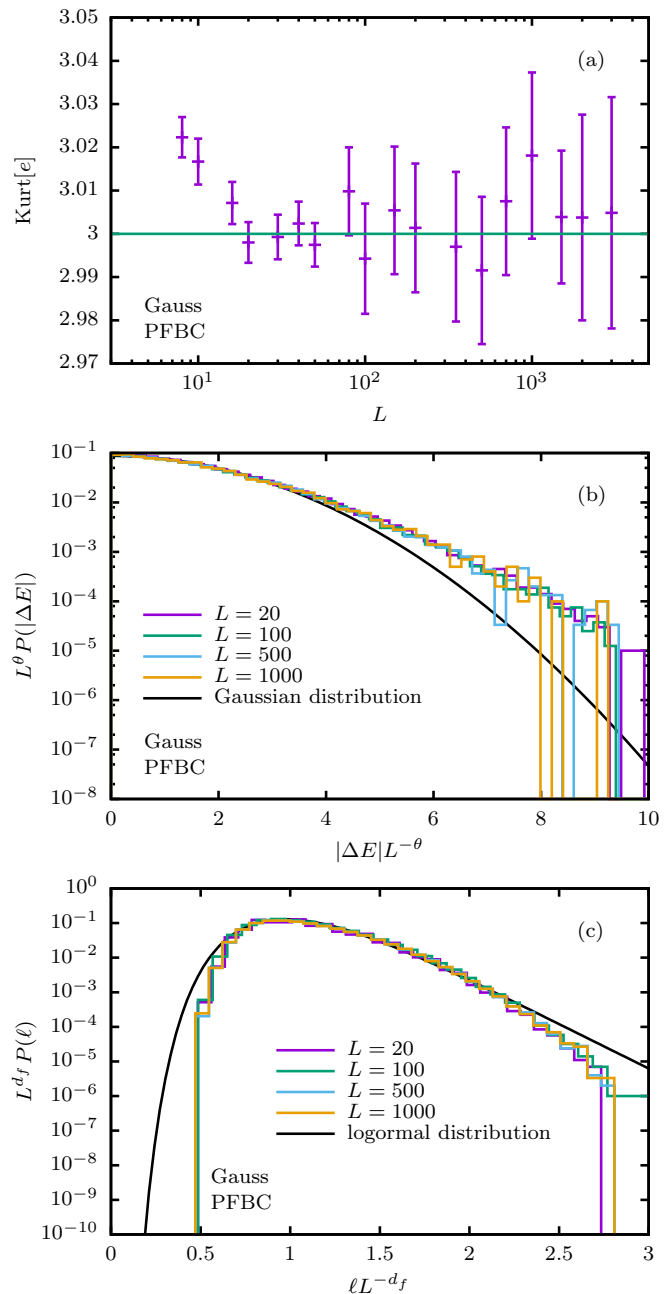

FIG. 8. (a) Scaling of the kurtosis Kurt[e] of the distribution of ground-state energies per spin for the Gaussian model with PFBC as a function of system size. For $L \geqslant 20$, it is consistent with the value Kurt[e] = 3 of a normal distribution. (b) Distribution of defect energies $|\Delta E|$ for the same model, rescaled with the expected asymptotic behavior $\propto L^\theta$ with $\theta = 0.2793$. The solid line shows a Gaussian distribution of the same mean and variance. (c) Distribution of domain-wall lengths ℓ for the PFBC Gaussian case, rescaled according to the limiting form $\propto L^{d_f}$ with $d_f = 1.273\,19$. The solid line represents a lognormal distribution fitted to the empirical data.

correlated and so the combined fluctuation is likely higher than the naive estimate [80,81]. The two PPBC estimates are fully consistent. The distribution of domain wall lengths is found to be clearly non-Gaussian, with a kurtosis that is consistent with Kurt[ℓ] = 3.656(4) for systems of size $L \geqslant L_{min} = 20$.

It was suggested in Ref. [41] that the distribution might be in fact lognormal. Our data for the distribution of ℓ for PFBC are shown in Fig. 8(c), together with a fit to a lognormal distribution. As is apparent, it describes the data reasonably well close to the mode, but there are significant deviations in the tails.

IV. RESULTS FOR BIMODAL COUPLINGS

For bimodal couplings there is a huge ground-state degeneracy. As has been demonstrated with numerical calculations [25,26] and also shown rigorously [82], this model even has a finite ground-state entropy, indicating that the number of ground states grows exponentially with system size. It turns out to be a challenge to fulfill the equilibrium requirement of ensuring that all such states are sampled with equal probability.

A. Uniform sampling of ground states

For the case of systems with ground-state degeneracies, the solution to the matching problem described in Sec. II C is not unique. There are several, possibly many solutions to the matching problem that have the same minimal weight. In practice, the implementation of the matching algorithm used will return an arbitrary solution out of this set, where the state chosen depends on the specific implementation of the algorithm used (for instance on the order in which nodes and edges are examined) and the state returned might or might not be reproducible between runs.[4] Clearly, this setup is not suitable for sampling such states with a prescribed probability weight.

One way of solving this problem and ensuring uniform sampling of states might be to break the degeneracy in a way such that each ground state is preferred the same number of times by a chosen procedure. If one examines a pair of ground states, one will find that they differ by the overturning of a set of disjoint, but singly connected clusters of spins. As, by definition, this procedure does not change the overall energy, this corresponds to a set of "free" spins [83]. The degeneracy can be lifted by adding some small perturbation to the bonds, i.e.,

$$J_{ij}(\kappa) = J_{ij} + \kappa\epsilon_{ij}, \tag{17}$$

with a continuous, symmetric distribution of the random variables ϵ_{ij}, a natural choice being the standard normal distribution, $\epsilon_{ij} \sim \mathcal{N}(0,1)$. As the spectrum of states for the bimodal model is gapped [26], if κ is chosen sufficiently small the ground state of the system with couplings $J_{ij}(\kappa)$ will also be a ground state of the system with $\kappa = 0$. Considering a cluster of free spins for a symmetric distribution of ϵ_{ij}, the sum of the noise terms ϵ_{ij} along the bonds on the cluster boundary will have either sign with the same probability of 1/2. Hence one half of the realizations of ϵ_{ij} should lead to this cluster being in one orientation and the other half to it being in the reversed orientation, implying uniform sampling of degenerate ground states. A similar approach was used in Refs. [43,84]. As we

discuss elsewhere [83], however, clusters that touch each other are not independent and hence the procedure leads to a strongly nonuniform distribution of sampled states.

Uniform sampling is achieved via a new technique based on a combination of combinatorial optimization in the form of the MWPM algorithm and Markov chain Monte Carlo [83]. We use MWPM to exactly determine the set of *rigid* clusters in the ground-state manifold, i.e., the set of connected regions such that the spins inside of them have the same relative orientation in all ground states. In a second step, we then perform a parallel tempering simulation [85] with updates that are a combination of flipping individual rigid clusters and a nonlocal cluster-update move [86]. Details of the procedure as well as benchmarks will be presented elsewhere [83].

B. Ground-state and defect energies

For the ground-state energy the presence of degeneracies and sampling bias is not relevant. We hence used the regular MWPM procedure to determine ground-state energies for pairs of samples with periodic and antiperiodic boundaries and the resulting defect energies. For these quantities we restricted our calculations to the case of PFBC as this allows for treating larger system sizes, but studies of PPBC would also be possible using the windowing technique. The range of system sizes and number of realizations for each size are summarized in the fourth column of Table V. The average ground-state energy per spin is shown in Fig. 9(a). Inspecting the general scaling ansatz (10) and taking into account that we expect $\theta = 0$ for this model (see below), we should only have analytical corrections proportional to $1/L$ and $1/L^2$ up to $O(L^{-3})$, and indeed we find a good fit ($Q = 0.18$) of this functional form for the range $L \geqslant L_{\min} = 20$, yielding

$$e_\infty = -1.401\,922(3).$$

This fit is shown together with the data in Fig. 9(a). No drift of e_∞ is visible on further increasing $L_{\min}$.

The defect energies resulting from this procedure are shown in Fig. 9(b), indicating that for this model $\langle|\Delta E|\rangle_J$ converges to a finite value instead of decaying away to zero. This is consistent with previous findings [14,57]. If we assume a power-law decay as prescribed by Eq. (13) and ignore the correction terms, i.e., we use a pure power-law form $\langle|\Delta E|\rangle_J = A_\theta L^\theta$, a good fit is achieved for $L \geqslant L_{\min} = 150$, resulting in $\theta = -0.012(4)$, marginally compatible with $\theta = 0$. Additionally, the modulus of θ systematically drops as $L_{\min}$ is increased. The defect energy in this case hence does not decay to zero, but attains a nonzero value in the thermodynamic limit. We therefore make the scaling ansatz

$$\langle|\Delta E|\rangle_J = \Delta E_\infty + B_\theta L^{-\omega}. \tag{18}$$

We find an excellent fit with $Q = 0.99$ already for $L_{\min} = 10$, resulting in

$$\Delta E_\infty = 0.960(5)$$

and $\omega = 0.67(4)$. An alternative fit form including analytic corrections proportional to $1/L$ and $1/L^2$ but omitting the $L^{-\omega}$ term is found to be of significantly lower quality.

Studying the distributions of both ground-state and defect energies, we again find a Gaussian shape for the ground-state

---

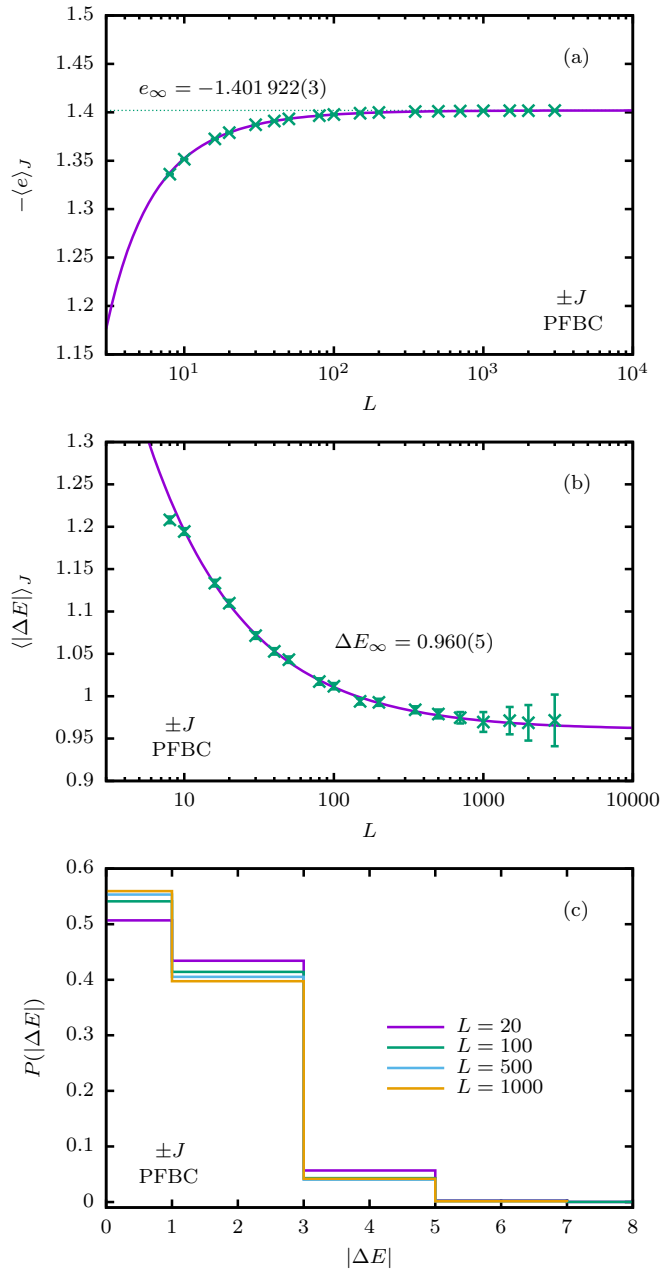[4]The energy of the state returned, on the other hand, is of course always the same.
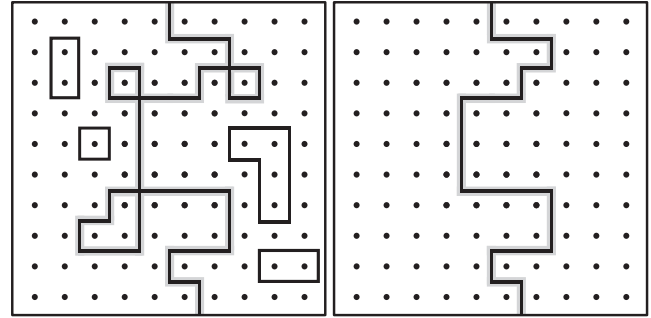
FIG. 10. (Left) Schematic representation of the set of dual bonds satisfying the condition (14) for the case of bimodal couplings. Besides the domain wall, it contains isolated loops enclosing free clusters of spins as well as bubbles of free spins attached to the domain wall. Removing the isolated free loops one arrives at the set $\mathcal{D}_{\text{long}}$, which we denote as the "long" domain wall. (Right) After the additional removal of bubbles one arrives at the set $\mathcal{D}_{\text{short}}$ of dual bonds comprising the "short" domain wall of the configuration.

FIG. 9. (a) Average ground-state energies for bimodal couplings and PFBC boundaries, together with a fit of the functional form (10) with $\theta = 0$ to the data for the range $L = 20, \ldots, 3000$. (b) Defect energies for systems with bimodal couplings and PFBC boundaries. Clearly, $\langle |\Delta E| \rangle_J$ converges to a nonzero value as $L \to \infty$, indicating that $\theta = 0$. The line shows a fit of the form $\langle |\Delta E| \rangle_J = \Delta E_\infty + B_\theta L^{-\omega}$ to the data with $L \geqslant L_{\min} = 10$ yielding $\Delta E_\infty = 0.960(5)$. (c) Probability distribution over disorder of the defect energies for the PFBC $\pm J$ model and different system sizes. For $L \to \infty$ the distribution approaches a limiting shape close to the $L = 1000$ case shown here.

energies, the kurtosis being compatible with that of a normal distribution for all system sizes studied. The standard deviation of the defect energy shows analogous behavior to $\langle |\Delta E| \rangle_J$, settling down at a finite value as $L \to \infty$. A fit of the form (18) yields an asymptotic $\sigma_\infty(\Delta E) = 1.1564(4)$ ($L_{\min} = 16$, $Q =$

0.41). The disorder distribution of defect energies is shown in Fig. 9(c), illustrating that it approaches a limiting shape as $L \to \infty$ in which about 57% of domain walls have zero energy, 38% have $\Delta E = 2$, 4% have $\Delta E = 4$, and higher defect energies occur in less than 1% of the cases.

C. Domain walls

The presence of free clusters of spins in the manifold of degenerate ground states complicates the identification of domain walls for the bimodal model [43]. A possible difference in configuration between the ground state for a disorder configuration with P boundaries and a ground state for the same realization with AP boundary conditions is schematically depicted in the left panel of Fig. 10. We see that in this case the set of domain-wall bonds satisfying condition (14), i.e., different relative orientations of spins at both ends for the P and AP configurations, does not only contain the actual domain wall but also a set of closed loops detached from the wall. These correspond to free clusters that can be overturned at zero energy cost and so happen to be in one orientation in the P ground state, but in the opposite orientation in the AP configuration. Conceptually, these bonds do not belong to the domain wall. We remove them by only counting the system spanning part of the set $\mathcal{D}$. We refer to the corresponding set, denoted as $\mathcal{D}_{\text{long}}$, as the "long" domain wall and its length as $\ell_{\text{long}} = |\mathcal{D}_{\text{long}}|$. Additionally, however, it is possible for such free clusters to be attached to the domain wall as is also depicted in the example of Fig. 10. Such "bubbles" attached to corners of the wall are somewhat arbitrary additions and removing them by only considering the shortest path in the set $\mathcal{D}$ connecting opposite ends of the system defines the reduced set $\mathcal{D}_{\text{short}}$ with $\ell_{\text{short}} = |\mathcal{D}_{\text{short}}|$. Clearly, we have that $\mathcal{D}_{\text{short}} \subseteq \mathcal{D}_{\text{long}} \subseteq \mathcal{D}$. Note that even after these removals the set $\mathcal{D}_{\text{short}}$ is not unique for a given bond configuration, and the additional degeneracy is connected to zero-energy loops that share (at least) one bond with the domain wall (instead of only sharing a corner) and hence can be interpreted as diversions of

the wall. In order to probe the equilibrium properties, we must sample from such walls with equal probability.

Regarding the sampling of domain-wall lengths for the bimodal model we have produced data from three different algorithms.

(1) Our implementation of the MWPM algorithm calculates a ground-state for each sample with both P and AP boundary conditions, and comparing these we can determine the lengths $\ell_{\rm short}$ and $\ell_{\rm long}$ of the related domain walls. It is clear that this does not correspond to a fair sampling of ground states, but the nature of the bias depends on internal details of the MWPM implementation [46] and is not clear on a physical level. This technique allows to treat large system sizes and we applied it to the data set of sizes $8 \leqslant L \leqslant 3000$ described in the third column of Table V. In the following, we denote this as the "matching" algorithm.

(2) The Gaussian noise technique described in Sec. IV A is designed to break the degeneracy in a systematic way. For each realization it only requires an additional run of the MWPM algorithm per boundary condition, and we hence applied it to the same set of samples with $8 \leqslant L \leqslant 3000$. As discussed in Sec. IV A it also does not provide uniform samples, however. This technique is referred to as "Gaussian noise" in the following.

(3) The new algorithm based on a cluster decomposition and parallel tempering outlined in Ref. [83] provides uniform samples, but it is much more demanding computationally, such that only smaller system sizes can be treated reliably. We have studied systems of edge lengths $L = 10, 16, 20, 24, 28, 32, 48, 64, 80, 100,$ and 128 for this method, using 1000 samples per size and producing ten independent ground-state configurations per sample. Data from this algorithm are labeled "uniform sampling."

Figure 11(a) shows the three data sets for the scaling of the lengths of short domain walls. On the scale of the domain-wall lengths themselves, all data appear to fall on top of each other, but a closer inspection reveals that this is in fact not the case. The data from uniform sampling show very clean scaling behavior and a pure power law $\langle \ell \rangle_J = A_\ell L^{d_{\rm f}}$ describes the data for $L \geqslant L_{\rm min} = 16$ well. No drift of the exponent value is observed on omitting further values on the small-L side. The fractal dimension is estimated from this fit as

$$d_{\rm f} = 1.279(2)$$

with $Q = 0.33$. As the inset of Fig. 11(a) shows, there are statistically significant deviations of the data from the other two sampling techniques from this result. The samples generated by the Gaussian noise technique show clean scaling as well, but with a significantly larger exponent $d_{\rm f} = 1.323(3)$ ($L_{\rm min} = 16, Q = 0.86$). The data from the matching approach alone, on the other hand, show somewhat inconsistent behavior for successive system sizes, and they are compatible with a pure power law only for $L \geqslant L_{\rm min} = 80$, yielding $d_{\rm f} = 1.2802(5)$ ($Q = 0.18$). This slightly unsteady statistical behavior is probably connected to the fact that the matching method does not use a stochastic sampling technique, and due to internal design decisions the behavior of the algorithm might change discontinuously at certain system sizes. Somewhat surprisingly, however, the results for the pure matching technique are closer to the correct result represented by uniform sampling than
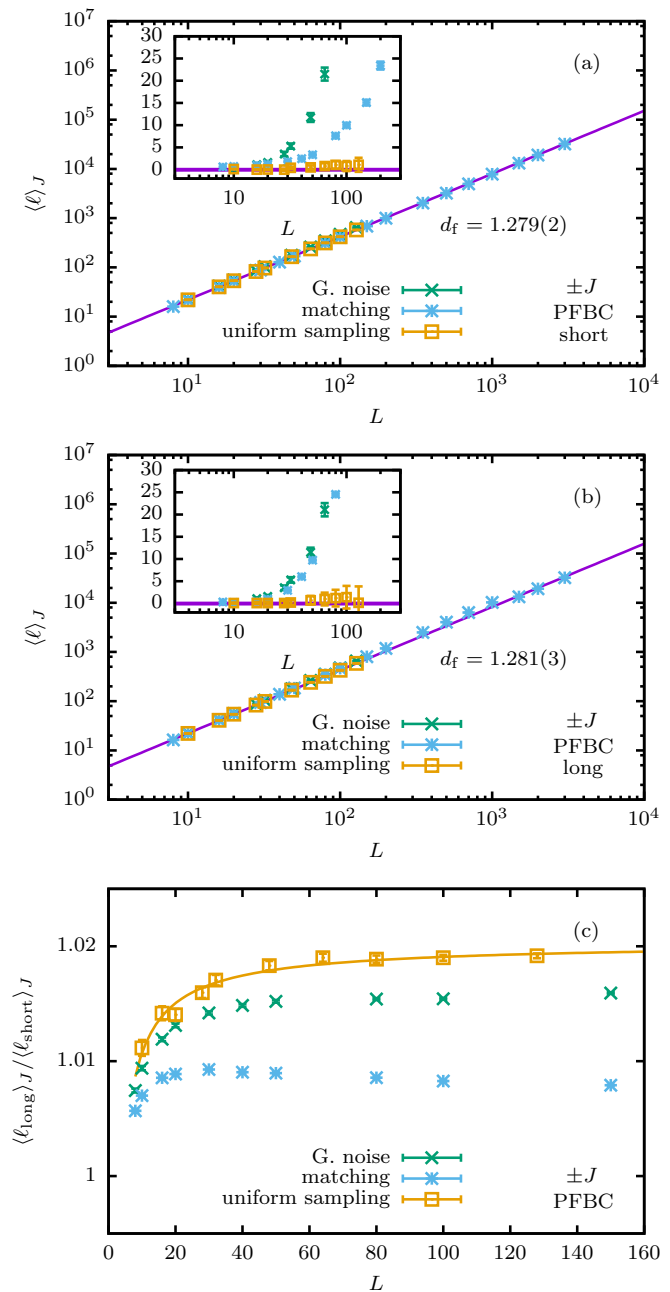

FIG. 11. (a) Average length $\langle \ell_{\rm short} \rangle_J$ of the short domain wall for the bimodal model as a function of linear system size L for the three different algorithms employed. The inset shows the deviation of each data set from the fit of the power law $\langle \ell \rangle_J = A_\ell L^{d_{\rm f}}$ to the uniform sampling data for $L \geqslant L_{\rm min} = 16$, which results in $d_{\rm f} = 1.279(2)$ ($Q = 0.33$). (b) Average length $\langle \ell_{\rm long} \rangle_J$ of the long domain walls for the different algorithms. The inset shows the deviation of each data set from the fit of a pure power law to the uniform data, yielding $d_{\rm f} = 1.281(3)$ for $L_{\rm min} = 16$ ($Q = 0.97$). (c) Ratio of the average lengths of long and short domain walls as estimated from the different algorithms. In all cases, the ratio approaches a constant, in line with the identical estimates of fractal dimension for $\ell_{\rm short}$ and $\ell_{\rm long}$.

the samples produced by Gaussian noise, see also the inset of Fig. 11(a).

We move on to considering the results for the long domain walls. The data are summarized in Fig. 11(b). While for each
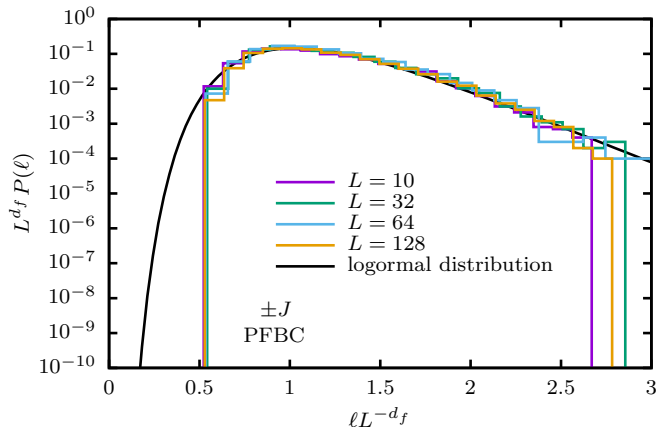
FIG. 12. Distribution of the lengths ℓ_{long} of the long domain walls for $\pm J$ couplings and PFBC boundaries as resulting from the uniform sampling approach. The rescaling of the axes is with respect to the fractal dimension $d_f = 1.281(3)$ estimated from the data in Fig. 11.

data set, the values of $\langle \ell_{\text{long}} \rangle_J$ are somewhat larger than those of $\langle \ell_{\text{short}} \rangle_J$ the relative behavior of the three data sets for the long domain walls is very similar to that found for the short walls. From the uniform sampling data, a pure power-law fit for $L_{\text{min}} = 16$ yields $d_f = 1.281(3)$ ($Q = 0.97$), which is statistically consistent with the result from the short domain walls. For comparison, matching and Gaussian noise yield $d_f = 1.2797(5)$ and $d_f = 1.325(3)$, respectively, for the same ranges that were used for the short walls. It hence appears that for the scaling of domain-wall length with system size, there is no difference between the short and long definitions of domain walls. This impression is corroborated by the data shown in Fig. 11(c) of the ratios of long and short lengths of domain walls, averaged over disorder, for the three different techniques. It is clear that this ratio settles down to a finite value as $L \to \infty$, and a fit of the functional form $\langle \ell_{\text{long}}/\ell_{\text{short}} \rangle_J = \kappa + A_\kappa L^{-\omega}$ to the uniform sampling data yields $\kappa = 1.021(6)$ and $\omega = 0.85(16)$ with $Q = 0.18$ ($L_{\text{min}} = 10$).

It is worthwhile to compare these estimates of the fractal dimension to those found previously: Melchert and Hartmann [41] used combinatorial optimization methods to find minimal and maximal domain walls in the manifold of degenerate ground-state pairs, yielding lower and upper bounds for d_f, namely $1.095(2) \leqslant d_f \leqslant 1.395(3)$. Our estimates are clearly compatible with these, and it is interesting to note that the actual value is much closer to the upper than to the lower limit, which corresponds to almost flat walls. Risau-Gusman and Romá [43] estimate $d_f = 1.323(3)$ using nonuniform sampling resulting from employing the bare MWPM algorithm; this is compatible with our "matching" results, but too large compared to the unbiased estimate from uniform sampling. Studying domain walls in a hexagonal lattice, Weigel and Johnston [42] find $d_f = 1.283(11)$, but again not using unbiased sampling. Analyzing the behavior of the ground-state entropy, Fisch [87] estimates $d_f = 1.22(1)$, which is strongly incompatible with our results, which could be a sign of the relation $d_f = 2\theta_S$ on which Fisch's estimate is based, where θ_S is the scaling exponent of the ground-state entropy, not being valid in two dimensions.

We finally tend to the distribution of domain-wall lengths for this case. As is illustrated in Fig. 12 for the long domain walls, these follow the scaling form $P(\ell) = L^{d_f} \hat{P}(\ell L^{-d_f})$ already observed for the case with Gaussian couplings, cf. Fig. 8(c), where now $d_f = 1.281(3)$. The fit to a log-normal distribution also shown in Fig. 12 works quite well over the full range of the distribution, in contrast to the case of Gaussian couplings, where deviations could be seen in the right tail, cf. Fig. 8(c). Very similar results are obtained for the distribution of short domain walls also (not shown).

V. CONCLUSIONS

We used an exact algorithm based on minimum-weight perfect matching to calculate ground states for the square-lattice Ising spin glass with Gaussian and bimodal couplings and lattice sizes of up to $10\,000 \times 10\,000$ (10^8) spins, employing periodic boundary conditions in one direction and free boundaries in the other. For systems with fully periodic boundaries, we developed a quasi-exact algorithm that can find true ground states with arbitrarily high probability and a computational effort that is a constant time larger than for the planar graphs, and we used it to study systems of up to $3\,000 \times 3\,000$ spins. Our estimates of the ground-state energies $e_\infty = -1.314\,787\,6(7)$ (Gaussian model) and $e_\infty = -1.401\,922(3)$ (bimodal model) are compatible with, but up to 100 times more precise than the estimates in the careful study of Ref. [55] using exact ground-state methods and the recent work Ref. [88] using Monte Carlo. For Gaussian couplings, we also determined the spin-stiffness exponent and the fractal dimension of domain walls with unprecedented precision, yielding $\theta = -0.2793(3)$ and $d_f = 1.273\,19(9)$. These estimates are one to two orders of magnitude more precise than previous results, see the data collected in Table I. We note that this value is also consistent with the most recent estimate of $1/\nu = -\theta = 0.283(6)$ in Ref. [11], but the zero-temperature result has tenfold increased precision. For bimodal couplings, we find $\theta = 0$, in agreement with previous studies. Due to the large degeneracy of the ground state for bimodal couplings, methods based on matching do not allow to sample states with the proper statistical weight, and as a result unbiased estimates of the domain-wall fractal dimension have not been possible previously. Using a newly developed algorithm [83] allowed us to sample exact ground states for this case uniformly, here up to system size $L = 128$. The resulting estimates of the fractal dimension, $d_f = 1.279(2)$ and $d_f = 1.281(3)$ for "short" and "long" domain walls, respectively, are marginally consistent with d_f for the Gaussian couplings, the deviation being 3 and 4 standard deviations, respectively.

In 2006, Amoruso *et al.* [38] used results from stochastic Loewner evolution (SLE) to conjecture that the 2D spin glass with Gaussian couplings is described by a nonunitary conformal field theory with central charge $c < -1$, related to the SLE parameter κ as [89] $c = (6 - \kappa)(3\kappa - 8)/\kappa$, and they numerically determined a value $\kappa \approx 2.1$. Further, it was assumed that the scaling dimension $x_t = d - y_t = d - 1/\nu = d + \theta = 2 + \theta$ of the energy operator should be represented in the corresponding Kac table [90], and a numerically close value was found in tentatively identifying $x_t = 2\Delta_{1,2} = (6 - \kappa)/\kappa$. Together with the relation $d_f = 1 + \kappa/8$ for the fractal

dimension, this yields the equation [38]

$$d_{\mathrm{f}} = 1 + \frac{3}{4(3+\theta)}. \tag{19}$$

We note that additional to the assumption of a CFT representation, the identification of conformal weights with items in the Kac table is only supposed to work for rational values of κ, which does not appear to be the case here. Equation (19) was found to be consistent with previous estimates of θ and d_{f} [38]. Our most accurate results are for PFBC boundaries. The corresponding estimate $d_{\mathrm{f}} = 1.273\,19(9)$ would imply via Eq. (19) that $\theta = -0.2546(9)$ which does not seem consistent with the estimate $\theta = -0.2793(3)$ from the defect energies. More systematically, if (19) is to hold, the difference

$$d_{\mathrm{f}} - 1 - \frac{3}{4(3+\theta)} = -0.00247(9)$$

must be consistent with zero. Here, we used the estimates for d_{f} and θ from PFBC and standard error propagation [91]. The difference from zero corresponds to about 27 standard deviations, so based on the usual confidence limits one would need to reject the hypothesis that our data are consistent with (19). This neglects the fact, however, that our estimates for d_{f} and θ are correlated as they are derived from the same set of disorder realizations [81]. To correct for this effect, we divided the disorder samples for PFBC such that one half is used to estimate $\theta = -0.2795(3)$ ($Q = 0.47$) and the other half is used to estimate $d_{\mathrm{f}} = 1.273\,22(12)$ ($Q = 0.32$) using the same fit functions and ranges as for the full data set. With these estimates, we find

$$d_{\mathrm{f}} - 1 - \frac{3}{4(3+\theta)} = -0.00246(12),$$

where the deviation from zero is still about 20 standard deviations, corresponding to the expected reduction by halving the statistics, so the correlation effect appears to be weak. As an alternative analysis, we also attempted to perform a simultaneous fit of power laws to the scaling of $|\Delta E|$ and ℓ while enforcing the relation (19) between the scaling exponents. Independent of whether we use the full or the split data set, a fit quality $Q > 0.01$ is only achieved for $L_{\min} \geqslant 1000$, which is way above the range of lattice sizes where scaling corrections are visible above the statistical errors (recall that both the defect energies and domain-wall lengths are fully consistent statistically with pure power-laws for $L > L_{\min} = 40$). The conclusions from considering the independent data set for PPBC are similar, with the deviation from Eq. (19) being $-0.00231(47)$, corresponding to five standard deviations. The values for the deviations for PFBC and PPBC are statistically consistent, the appearance of better consistency for PPBC is due to the smaller statistics there. While it is always difficult to reject or confirm an exact (but nonrigorous) relation based on numerics, it appears safe to say that our data do not appear to be consistent with Eq. (19).[5] It is worthwhile to note that, on the other hand, our values for θ and d_{f} are fully consistent with previous estimates, cf. the data compiled in Table I, and it is only due to the increased accuracy resulting from the bigger systems and larger numbers of disorder samples considered here that the inconsistency with Eq. (19) arises. Our results for the fractal dimension of the bimodal model are marginally consistent with those for the Gaussian model, and it remains an interesting question for further studies whether universality between the two models holds in this respect.

---

[5]While we tried to take careful account of scaling corrections by including additional terms in the fit functions and/or monitoring the dependence of the results on the choice of $L_{\min}$, it is not possible to completely exclude the possibility of spurious systematic corrections leading to the observed deviations from Eq. (19).

---

[1] N. Kawashima and H. Rieger, in *Frustrated Spin Systems*, edited by H. T. Diep (World Scientific, Singapore, 2005), Chap. 9, p. 491.

[2] K. Binder and A. P. Young, Rev. Mod. Phys. **58**, 801 (1986).

[3] H. Nishimori, *Statistical Physics of Spin Glasses and Information Processing* (Oxford University Press, Oxford, 2001).

[4] D. X. Viet and H. Kawamura, Phys. Rev. Lett. **102**, 027202 (2009).

[5] L. A. Fernández, V. Martín-Mayor, S. Perez-Gaviro, A. Tarancón, and A. P. Young, Phys. Rev. B **80**, 024422 (2009).

[6] D. X. Viet and H. Kawamura, Phys. Rev. Lett. **105**, 097206 (2010).

[7] A. Sharma and A. P. Young, Phys. Rev. B **83**, 214405 (2011).

[8] F. Beyer, M. Weigel, and M. A. Moore, Phys. Rev. B **86**, 014431 (2012).

[9] M. Hasenbusch, A. Pelissetto, and E. Vicari, J. Stat. Mech.: Theory Exp. (2008) L02001.

[10] M. Ohzeki and H. Nishimori, J. Phys. A **42**, 332001 (2009).

[11] L. A. Fernández, E. Marinari, V. Martín-Mayor, G. Parisi, and J. J. Ruiz-Lorenzo, Phys. Rev. B **94**, 024402 (2016).

[12] F. Parisen Toldin, A. Pelissetto, and E. Vicari, J. Stat. Phys. **135**, 1039 (2009).

[13] C. K. Thomas and H. G. Katzgraber, Phys. Rev. E **84**, 040101 (2011).

[14] A. K. Hartmann and A. P. Young, Phys. Rev. B **64**, 180404 (2001).
[15] T. Jörg, J. Lukic, E. Marinari, and O. C. Martin, Phys. Rev. Lett. **96**, 237205 (2006).
[16] F. Romá, S. Risau-Gusman, A. J. Ramirez-Pastor, F. Nieto, and E. E. Vogel, Phys. Rev. B **82**, 214401 (2010).
[17] C. K. Thomas, D. A. Huse, and A. A. Middleton, Phys. Rev. Lett. **107**, 047203 (2011).
[18] F. Parisen Toldin, A. Pelissetto, and E. Vicari, Phys. Rev. E **84**, 051116 (2011).
[19] T. Jörg and F. Krzakala, J. Stat. Mech.: Theory Exp. (2012) L01001.
[20] N. Jinuntuya and J. Poulter, J. Stat. Mech.: Theory Exp. (2012) P01010.
[21] P. H. Lundow and I. A. Campbell, Phys. Rev. E **93**, 022119 (2016).
[22] F. Barahona, J. Phys. A **15**, 3241 (1982).
[23] I. Bieche, R. Maynard, R. Rammal, and J. P. Uhry, J. Phys. A **13**, 2553 (1980).
[24] A. K. Hartmann and A. P. Young, Phys. Rev. B **66**, 094419 (2002).
[25] J. A. Blackman and J. Poulter, Phys. Rev. B **44**, 4374 (1991).
[26] L. Saul and M. Kardar, Phys. Rev. E **48**, R3221 (1993).
[27] A. Galluccio, M. Loebl, and J. Vondrák, Phys. Rev. Lett. **84**, 5924 (2000).
[28] C. K. Thomas and A. A. Middleton, Phys. Rev. E **80**, 046708 (2009).
[29] J. G. Propp and D. B. Wilson, Rand. Struct. Alg. **9**, 223 (1996).
[30] D. B. Wilson, in *Proceedings of the Eighth Annual ACM-SIAM Symposium on Discrete Algorithms (SODA)* (ACM, New York, 1997), pp. 258–267.
[31] C. Chanal and W. Krauth, Phys. Rev. Lett. **100**, 060601 (2008).
[32] W. L. McMillan, J. Phys. C **17**, 3179 (1984).
[33] A. J. Bray and M. A. Moore, in *Heidelberg Colloquium on Glassy Dynamics*, edited by J. L. van Hemmen and I. Morgenstern (Springer, Heidelberg, 1987), p. 121.
[34] D. S. Fisher and D. A. Huse, Phys. Rev. B **38**, 386 (1988).
[35] A. K. Hartmann and M. A. Moore, Phys. Rev. Lett. **90**, 127201 (2003).
[36] A. K. Hartmann, Phys. Rev. B **77**, 144418 (2008).
[37] A. J. Bray and M. A. Moore, Phys. Rev. Lett. **58**, 57 (1987).
[38] C. Amoruso, A. K. Hartmann, M. B. Hastings, and M. A. Moore, Phys. Rev. Lett. **97**, 267202 (2006).
[39] D. Bernard, P. Le Doussal, and A. A. Middleton, Phys. Rev. B **76**, 020403 (2007).
[40] H. Khoshbakht, J. D. Stevenson, and M. Weigel (unpublished).
[41] O. Melchert and A. K. Hartmann, Phys. Rev. B **76**, 174411 (2007).
[42] M. Weigel and D. A. Johnston, Phys. Rev. B **76**, 054408 (2007).
[43] S. Risau-Gusman and F. Romá, Phys. Rev. B **77**, 134435 (2008).
[44] G. Pardella and F. Liers, Phys. Rev. E **78**, 056705 (2008).
[45] C. K. Thomas and A. A. Middleton, Phys. Rev. B **76**, 220406 (2007).
[46] V. Kolmogorov, Math. Prof. Comp. **1**, 43 (2009).
[47] C. K. Thomas, O. L. White, and A. A. Middleton, Phys. Rev. B **77**, 092415 (2008).
[48] W. L. McMillan, Phys. Rev. B **29**, 4026 (1984).
[49] M. Palassini and A. P. Young, Phys. Rev. B **60**, R9919 (1999).
[50] A. J. Bray and M. A. Moore, J. Phys. C **17**, L463 (1984).
[51] H. Rieger, L. Santen, U. Blasum, M. Diehl, M. Jünger, and G. Rinaldi, J. Phys. A **29**, 3939 (1996).
[52] A. A. Middleton, Phys. Rev. B **63**, 060202 (2001).
[53] A. K. Hartmann, A. J. Bray, A. C. Carter, M. A. Moore, and A. P. Young, Phys. Rev. B **66**, 224401 (2002).
[54] A. C. Carter, A. J. Bray, and M. A. Moore, Phys. Rev. Lett. **88**, 077201 (2002).
[55] I. A. Campbell, A. K. Hartmann, and H. G. Katzgraber, Phys. Rev. B **70**, 054429 (2004).
[56] O. Melchert and A. K. Hartmann, Comput. Phys. Commun. **182**, 1828 (2011).
[57] C. Amoruso, E. Marinari, O. C. Martin, and A. Pagnani, Phys. Rev. Lett. **91**, 087201 (2003).
[58] G. Toulouse, Commun. Phys. **2**, 115 (1977).
[59] J. Edmonds, J. Res. Natl. Bur. Stand. B **69**, 125 (1965).
[60] Spin-glass server, http://www.informatik.uni-koeln.de/spinglass/.
[61] M. Weigel, Phys. Rev. E **76**, 066706 (2007).
[62] F. Liers, M. Jünger, G. Reinelt, and G. Rinaldi, Computing exact ground states of hard ising spin glass problems by branch-and-cut, in *New Optimization Algorithms in Physics*, edited by A. Hartmann and H. Rieger (Wiley VCH, Weinheim, 2004).
[63] J. P. Bouchaud, F. Krzakala, and O. C. Martin, Phys. Rev. B **68**, 224404 (2003).
[64] M. Weigel and M. J. P. Gingras, Phys. Rev. B **77**, 104437 (2008).
[65] V. Privman, in *Finite Size Scaling and Numerical Simulation of Statistical Systems*, edited by V. Privman (World Scientific, Singapore, 1990), pp. 1–98.
[66] J. Wehr and M. Aizenman, J. Stat. Phys. **60**, 287 (1990).
[67] J. R. Banavar and M. Cieplak, Phys. Rev. Lett. **48**, 832 (1982).
[68] J. M. Kosterlitz and N. Akino, Phys. Rev. Lett. **82**, 4094 (1999).
[69] M. Weigel and M. J. P. Gingras, Phys. Rev. Lett. **96**, 097206 (2006).
[70] M. Palassini and A. P. Young, Phys. Rev. Lett. **85**, 3017 (2000).
[71] F. Krzakala and O. C. Martin, Phys. Rev. Lett. **85**, 3013 (2000).
[72] C. M. Newman and D. L. Stein, Phys. Rev. Lett. **87**, 077201 (2001).
[73] E. Marinari and G. Parisi, Phys. Rev. B **62**, 11677 (2000).
[74] G. K. Savvidy and N. G. Ter-Arutyunyan-Savvidy, J. Comp. Phys. **97**, 566 (1991).
[75] K. G. Savvidy, Comput. Phys. Commun. **196**, 161 (2015).
[76] P. L'Ecuyer and R. Simard, ACM Trans. Math. Softw. **33**, 22 (2007).
[77] M. Matsumoto and T. Nishimura, ACM Trans. Model. Comput. Simul. **8**, 3 (1998).
[78] V. Dotsenko, Y. Holovatch, M. Dudka, and M. Weigel, Phys. Rev. E **95**, 032118 (2017).
[79] T. Aspelmeier and M. A. Moore, Phys. Rev. Lett. **90**, 177201 (2003).
[80] M. Weigel and W. Janke, Phys. Rev. Lett. **102**, 100601 (2009).
[81] M. Weigel and W. Janke, Phys. Rev. E **81**, 066701 (2010).
[82] J. E. Avron, G. Roepstorff, and L. S. Schulman, J. Stat. Phys. **26**, 25 (1981).
[83] H. Khoshbakht and M. Weigel (unpublished).
[84] M. Cieplak and J. R. Banavar, J. Phys. A **23**, 4385 (1990).
[85] K. Hukushima and K. Nemoto, J. Phys. Soc. Jpn. **65**, 1604 (1996).
[86] J. Houdayer, Eur. Phys. J. B **22**, 479 (2001).
[87] R. Fisch, J. Stat. Phys. **130**, 561 (2008).

[88] D. J. Perez-Morelo, A. J. Ramirez-Pastor, and F. Romá, Physica A (Amsterdam) **391**, 937 (2012).

[89] M. Henkel and D. Karevski, *Conformal invariance: An introduction to Loops, Interfaces and Stochastic Loewner Evolution*, Lecture Notes in Physics Vol. 853 (Springer, Berlin, 2012).

[90] M. Henkel, *Conformal Invariance and Critical Phenomena* (Springer, Berlin, Heidelberg, New York, 1999).

[91] S. Brandt, *Data Analysis: Statistical and Computational Methods for Scientists and Engineers*, 3rd ed. (Springer, Berlin, 1998).

[92] A. P. Young, *Everything You Wanted to Know about Data Analysis and Fitting but Were Afraid to Ask*, Springer Briefs in Physics (Springer, Berlin, 2015).

[93] M.-S. Vaezi, Z. Nussinov, G. Ortiz, and M. Weigel, arXiv:1712.08602.